[Frontiers in Bioscience, Landmark, 21, 719-743, January 1, 2016]

Higher cardiogenic potential of IPSCs derived from cardiac versus skin stromal cells

Viviana Meraviglia[1,2], Jianyan Wen[3], Luca Piacentini[4], Giulia Campostrini[5], Cheng Wang[3], Maria Cristina Florio[2], Valerio Azzimato[1,6], Lorenzo Fassina[7], Martin Langes[8], Johnson Wong[3], Michele Miragoli[9,10], Carlo Gaetano[11], Giulio Pompilio[1,12], Andrea Barbuti[5,13], Dario DiFrancesco[5], Deborah Mascalzoni[2], Peter P. Pramstaller[2], Gualtiero I. Colombo[4], Huei-Sheng Vincent Chen[3,14], Alessandra Rossini[2,12]

[1]Laboratory of Vascular Biology and Regenerative Medicine Centro Cardiologico Monzino IRCCS, Milano, 20138 Italy, [2]Center for Biomedicine, European Academy Bozen/Bolzano (EURAC) (affiliated institute of the University of Lübeck), Bolzano, 39100 Italy, [3]Del E. Webb Center for Neuroscience, Aging & Stem Cell Research, Sanford-Burnham-Prebys Medical Discovery Institute, La Jolla, California 92037, USA, [4]Laboratory of Immunology and Functional Genomics, Centro Cardiologico Monzino IRCCS, Milano, 20138 Italy, [5]The PaceLab, Department of Biosciences, University of Milano, Milano, 20133 Italy, [6]Department of Pharmacological and Biomolecular Sciences, University of Milano, Milano, 20133 Italy, [7]Department of Electrical, Computer and Biomedical Engineering, University of Pavia, Pavia, 27100 Italy, [8]Laboratorio Specialistico di Ematologia, Ospedale Centrale di Bolzano, Azienda Sanitaria dell'Alto Adige, Bolzano, 39100 Italy, [9]CERT, Center of Excellence for Toxicological Research, INAIL, ex ISPESL, University of Parma, Parma, 43125 Italy, [10]Humanitas Clinical and Research Center, Rozzano (Milano), 20089 Italy, [11]Division of Cardiovascular Epigenetics, Department of Cardiology, Goethe University, Frankfurt am Main, 60590 Germany, [12]Department of Clinical Sciences and Community Health, University of Milano, Milano, 20122 Italy, [13]Centro Interuniversitario di Medicina Molecolare e Biofisica Applicata (CIMMBA), University of Milano, Milano, 20133 Italy, [14]Departments of Medicine/Cardiology, University of California-San Diego (UCSD), La Jolla, California 92037, USA

TABLE OF CONTENTS

1. ABSTRACT

Prior studies have demonstrated that founder cell type could influence induced pluripotent stem cells (iPSCs) molecular and developmental properties at early passages after establishing their pluripotent state. Herein, we evaluated the persistence of a functional memory related to the tissue of origin in iPSCs from syngeneic cardiac (CStC) *vs* skin stromal cells (SStCs). We found that, at passages greater than 15, iPSCs from cardiac stromal cells (C-iPSCs) produced a higher number of beating embryoid bodies than iPSCs from skin stromal cells (S-iPSCs). Flow cytometry analysis revealed that dissected beating areas from C-iPSCs exhibited more Troponin-T positive cells compared to S-iPSCs. Beating areas derived from C-iPSCs displayed higher expression of cardiac markers, more hyperpolarized diastolic potentials, larger action potential amplitude and higher contractility than beaters from skin. Also, different microRNA subsets were differentially modulated in CStCs *vs* SStCs during the reprogramming process, potentially accounting for the higher cardiogenic potentials of C-iPSCs *vs* S-iPSCs. Therefore, the present work supports the existence of a founder organ memory in iPSCs obtained from the stromal component of the origin tissue.

2. INTRODUCTION

The invention of Induced Pluripotent Stem Cell (iPSC) technology opened a new era for patient-specific personalized medicine (1). iPSCs are also the most important potential source of human cardiomyocytes for basic research, drug screening, disease modeling, and regenerative medicine (1, 2). iPSCs closely resemble human embryonic stem cells (hESCs) in terms of their morphology and differentiation ability into cells of the three germ layers, yet their use poses less ethical concerns than hESCs. Many somatic cell types have been successfully reprogrammed into iPSCs by expression of four exogenous transcription factors (*i.e.,* Oct3/4, Sox-2, c-Myc, and Klf4), including skin fibroblasts, blood cells, keratinocytes, bone marrow mesenchymal stem cells, adipose stromal cells, hair follicles, and dental pulp cells (3-9). Although early reports suggests that iPSCs display epigenetic and transcriptional similarities to hESCs, recent evidence indicates that iPSCs can retain a memory of their tissue of origin, such as preserving the DNA methylation signature typical of their donor cells particularly at early cell passages after pluripotency induction (5, 10).

Researchers have successfully reprogrammed neonatal murine cardiomyocytes (CMs) and human Sca-1 positive cardiac progenitors to iPSCs, which displayed a higher propensity to re-differentiate into CMs than iPSCs derived from syngeneic cardiac, tail and skin fibroblasts (11-13). Nevertheless, no one has to date demonstrated that fibroblasts from different tissues can generate iPSCs with specific differentiation ability. We recently showed that, compared to stromal cells derived from bone marrow, cardiac stromal cells (CStCs), even in their original state, exhibited higher expression of cardiac mesoderm-related genes and had a higher propensity to differentiate towards the myocardial lineage both *in vitro* and *in vivo* (14). Here, we find that at passages greater than 15, iPSCs derived from human CStCs, when compared to iPSCs derived from syngeneic skin stromal cells (SStCs), retain a differentiation memory of their founder organ, showing higher ability to generate cardiomyocytes although deriving from the stromal component of the tissue and not from the parenchyma. Of note, we also found a subset of microRNAs that, being differentially modulated in cardiac *vs* skin stromal cells during the pluripotency induction process, can be potentially associated with the epigenetic regulation of higher cardiogenic potentials of iPSCs from CStCs *vs* SStCs.

3. MATERIALS AND METHODS

3.1. Ethics statement

Human fetal skin (SStC) and cardiac (CStC) stromal cells were isolated from discarded right atrial tissues and skin of the same aborted fetuses of healthy pregnant women after signed informed consent from University of California-San Diego and iPSCs were generated at the Sanford Burnham Medical Research Institute. Approved research protocols from respective Institutional Review Boards or Institute Ethical committee at each institution were obtained prior to this study. Experiments were conducted in accordance to the principles expressed in the Declaration of Helsinki. All data were collected and analyzed anonymously.

3.2. Isolation and culture of skin and cardiac fetal stromal cells

Briefly, heart and skin tissues were minced into small pieces (size between 2-4 mm^2) and digested with 0.25 percent of trypsin-EDTA for 5 minutes at 37°C. After digestion, the supernatant was discarded and the tissue pieces were placed on culture dishes in standard growth medium (GM), composed of Iscove's Modified Dulbecco's Medium (IMDM, Lonza) supplemented with 20 percent of fetal bovine serum (FBS, Hyclone), 10 ng/ml basic Fibroblast Growth Factor (bFGF, R&D System), 10,000 U/ml Penicillin/Streptomycin (Invitrogen), 20 mM L-Glutamine (Sigma-Aldrich). Fibroblasts started to migrate out of the explants in 7-10 days and reach 90 percent of confluence in 2-3 weeks. The stromal cell population was sub-selected by culturing fibroblasts on the plastic surface of a 12-well plate for 30-60 minutes and only the most adhesive cells were retained for further passages and subsequent characterization.

3.3. Flow cytometry

Cells were detached with 0.02 percent of EDTA solution (Sigma-Aldrich) and incubated with FITC/PE/

Table 1. List and working concentrations of primary antibodies

Antibody	Manufacturer	Dilution
Rabbit anti human Nkx2.5	Abcam	1:1000
Mouse anti alpha-myosin heavy chain	Abcam	1:500
Mouse anti MDR-1	Sigma	1:250
Mouse anti human SSEA4	Millipore	1:250
Mouse anti humanTRA-1-60	Millipore	1:250
Mouse anti human TRA-1-81	Millipore	1:250
Rabbit anti human Nanog	Santa Cruz Biotechnology	1:500
Rabbit anti human Oct 3/4	Santa Cruz Biotechnology	1:500
Mouse anti beta-tubulin Isotype III (Tuj1)	Sigma aldrich	1:200
Rabbit anti Sox-17	Millipore	1:100
Mouse anti smooth muscle actin	DAKO	1:100
Mouse anti alpha-actinin	Sigma Aldrich	1:100
Rabbit anti troponin I	Santa Cruz Biotechnology	1:250
Mouse anti GCN5	Abcam	1:500
Rabbit PCAF	Abcam	1:500
Mouse GAPDH	Santa Cruz Biotechnology	1:5000
Mouse anti human beta-tubulin	Cell signalling	1:4000

APC conjugated primary antibodies for 10 minutes at room temperature. The following antibodies were used: CD13, CD14, CD29, CD31, CD34, CD44, CD45, CD73, CD90, CD117, HLA-ABC, HLA-DR, Chondroitin sulfate and Nestin (BD Biosciences); VEGFR2, CD105, CD144 and CD146 (R&D Systems). Embryoid bodies and dissected beating areas were dissociated at single cell level with TrypLE for 10 minutes at 37°C and then fixed and permeabilized using BD Cytofix/Cytoperm (BD Biosciences), following the manufacturer's instructions. Cells were incubated with a primary antibody against Troponin-T (Tn-T, Abcam) for 30 minutes at 4°C and then with an APC-conjugated secondary antibody (Abcam) for 30 minutes at 4°C. Cells were incubated with the corresponding IgG isotype, conjugated with the same fluorochrome used for the primary antibody. Cells were analyzed using a FACSCalibur flow cytometer (BD Biosciences) equipped with Cell-Quest Software v2.4.

3.4. Evaluation of fetal cell plasticity towards the cardiovascular lineages

SStCs and CStCs were plated at a density of 5000 cells/cm^2 and exposed to the appropriate medium. The medium was changed twice a week. Cells were then analyzed for the acquisition of lineage-specific properties. Specifically, the appearance of cardiac precursor phenotype was assessed after a 7 day-treatment with an Epigenetic cocktail (EpiC) containing 5 mM all-trans retinoic acid (ATRA), 5 mM phenyl butyrate (PB), and 200 mM diethylenetriamine/nitric oxide (DETA/NO) (15, 16).

3.5. Western blot

SStCs and CStCs were lysed with Laemmli buffer containing phosphatase inhibitors (Roche). Total proteins were resolved by SDS-PAGE and transferred onto nitrocellulose membrane (Bio-Rad). Membranes were incubated overnight at 4°C with primary antibodies (Table 1) and then 1 hour at room temperature with the appropriate HRP-conjugated secondary antibody (Amersham-GE Healthcare). Each membrane was also probed with anti-beta-tubulin or anti-GAPDH to verify equal protein loading. Chemiluminescence detection was performed using ECL (Amersham-GE Healthcare). Densitometric analyses were performed using the NIH ImageJ software v1.43.67.

3.6. Generation and culture of iPSCs

IPSCs from SStCs and CStCs were generated using an integration-free episomal method as previously described, using pCXLE-EGFP, pCXLE-hOCT3/4-shp53-F, pCXLE-hSK, and pCXLE-hUL (Addgene) as episomal vectors (17, 18). Briefly, fetal StCs were electroporated using a Neon System (Invitrogen) with 1 microgram for each episomal vector and then plated onto a plastic tissue culture dish. Six days after the electroporation, transfected fibroblasts were trypsinized and plated onto Matrigel-coated dishes containing an irradiated mouse embryonic fibroblast (MEF) feeder layer in GM. One day later, the medium was changed to stem cell medium containing: knockout KO-DMEM (Gibco), 20 percent of KO-Serum Replacement (KOSR, Gibco), 1 mM NEAAs (Gibco), 10,000 U/ml Penicillin/Streptomycin (Invitrogen), 20 mM L-Glutamine (Sigma-Aldrich), 0.1 mM beta-mercaptoethanol (Gibco), and 10 ng/ml bFGF (R&D System). iPSC colonies were selected based on stem cell-like morphology at 18-20 days after transfection and expanded after manual micro-dissection by plating on Matrigel-coated dishes containing a MEF feeder layer.

3.7. Alkaline phosphatase assay

The expression of alkaline phosphatase was evaluated using the Alkaline Phosphatase Staining Kit (Stemgent), according to manufacturer's instructions.

3.8. Immunofluorescence

Cells were fixed with 4 percent of PFA for 10 minutes and permeabilized with 0.2 percent of Triton-100X (Sigma-Aldrich); then a blocking buffer (5% BSA in PBS) was added for 1 hour at room temperature. Primary antibodies for selected markers (Table 1) diluted in blocking buffer were added overnight at 4°C.

FITC and TRITC-conjugated secondary antibodies (Jackson Immunoresearch) were added for 1 hour at 37°C and nuclei were counterstained by DAPI. Slides were analyzed using an Axio Observer Z1 microscope, equipped with the Apotome system and the software Axiovision (Zeiss).

3.9. Cardiomyogenic differentiation

The cardiomyogenic differentiation protocol for iPSCs was performed as previously described (18, 19). Cardiomyogenic differentiation experiments were performed using three independent iPSC lines. In brief, iPSCs were differentiated as embryoid bodies (EBs) by detaching colonies from the MEF feeder using 1 mg/ml Collagenase IV (Gibco) for 5 minutes at 37 °C. EBs were maintained for six days in suspension culture in ultra-low attachment plates in EB media, composed of: KO-DMEM (Gibco) with 20 percent of FBS (Hyclone), 1 mM NEAAs (Gibco), 10,000 U/ml Penicillin/Streptomycin (Invitrogen), 20 mM L-Glutamine (Sigma-Aldrich), and 0.1 mM beta-mercaptoethanol (Gibco). At day 7, EBs were plated onto gelatin-coated dishes for better detection of beating foci. Beating clusters usually appeared at 10-12 days from the beginning of the differentiation protocol. Approximately at day 25 of EB differentiation, beating areas were manually micro-dissected to enrich the cardiomyocyte population, plated onto gelatin-coated plates, maintained in the same EB medium except for supplementation with only 2 percent of FBS (to avoid fibroblast over-growth) and used at day 30 and day 60 for RT-qPCR, immunofluorescence and electrophysiology analyses.

3.10. Electrophysiology

Electrophysiology recordings were performed on dissected spontaneously beating bodies as previously described with minor modifications (20). Spontaneously beating areas were manually dissected from the EBs and plated in 35 mm dishes with 0.1 percent of gelatin. After few days, necessary for the adhesion to the plate, the dishes were placed on the stage of an inverted microscope and superfused with a Tyrode solution pH 7.4 containing: 140 mM NaCl, 5.4 mM KCl, 1.8 mM $CaCl_2$, 1 mM $MgCl_2$, 5.5 mM D-glucose, and 5 mM Hepes-NaOH. Spontaneous action potentials were recorded from whole beating areas by the patch-clamp technique in current clamp mode using a whole-cell configuration. The patch pipette had a resistance of 5-8 MΩ when filled with the intracellular-like solution pH 7.2 containing: 130 mM K-aspartate, 10 mM NaCl, 5 mM EGTA-KOH, 2 mM $CaCl_2$, 2 mM $MgCl_2$, 2 mM ATP (Na-salt), 5 mM phosphocreatine, 0.1 mM GTP (Na-salt), and 10 mM Hepes-KOH. Temperature was kept at 36±1 °C. Isoproterenol (1 microM) was added to the Tyrode solution from a concentrated stock. Beating rates, maximum diastolic potential (MDP) and action potential amplitude were analyzed using Clampfit and Origin v9.0 software.

3.11. Evaluation of cardiac contraction parameters

In order to compare C-iPSCs and S-iPSCs, beating areas from the kinematic and dynamic perspective, evaluations of contractility (maximum velocity of contraction propagation within the beating areas), and contraction frequency were carried out as previously described (21). Briefly, video observations of 30 seconds were recorded by a CCD camera at 16 frames per second (Cool SnapTM EZ Photometrics). After that, the Video Spot Tracker (VST) program was used to track the motion of one or more spots in a video (http://cismm.cs.unc.edu/downloads). In each video, 4 spots or markers were systematically selected onto the first video frame. By starting the videos in VST, frame by frame, the program followed and registered the spatial-temporal coordinates x, y, and t for each marker. The coordinates x and y were expressed in (pixel), whereas the coordinate t in seconds (s). Moreover, using an algorithm based on the Matlab programming language (The MathWorks, Inc., Natick, MA), frame by frame and for each marker, kinematics and dynamics of the beating syncytia were studied, as previously described (21). The statistical differences between the observed measures were tested via Kruskal-Wallis test, followed by Dunn-Sidák correction, electing a significance level of 0.05; the results were expressed as median with 25^{th} and 75^{th} percentiles.

3.12. Real-time reverse transcription–polymerase chain reaction (RT-qPCR) analysis

Total RNA was extracted from StCs, iPSCs and EBs using TRIzol reagent (Invitrogen) following the manufacturer's instructions. Total RNA concentration and purity were evaluated by a NanoDrop 1000 spectrophotometer (Thermo Scientific), while RNA integrity was assessed with an Experion electrophoresis system using the RNA High Sense Analysis Kit (Bio-Rad). Only high quality RNAs, with A260/A280 and A260/A230 ratios > 1.8 and a RQI > 9.5, were used for subsequent investigations. 1 microgram of total RNA was reverse transcribed using Superscript III First-Strand Synthesis SuperMix (Invitrogen). cDNA was amplified by SYBR-GREEN quantitative PCR on an iQ5 Cycler (Bio-Rad). Primer sequences for all the genes tested are reported in Table 2. Individual miR expression was analyzed by using specific single-assay miR primers (Applied Biosystems). Assays used were for hsa-miR-1, hsa-miR-133a, hsa-miR-133b, hsa-miR-208, and U6 snRNA. Reverse-transcription and real-time PCR reactions were performed according to the manufacturer's instructions, using a 7900TH Real-Time PCR System (Applied Biosystems). Raw expression intensities were normalized using the Ct value of GAPDH and U6 snRNA, for genes and miRs respectively. A Ct value=40 was arbitrarily assigned to unexpressed genes/miRs. Relative quantitation was performed using the ΔΔCt method. Fold changes in gene expression were estimated as $2^{(-\Delta\Delta Ct)}$ (22).

Table 2. List of primers sequences 5'-3' for RT-qPCR

Primer	Sequence
c-MYC fw	5'-AGAAATGTCCTGAGCAATCACC-3'
c-MYC rev	5'-AAGGTTGTGAGGTTGCATTTGA-3'
KLF4 fw	5'-ATAGCCTAAATGATGGTGCTTGG-3'
KLF4 rev	5'- AACTTTGGCTTCCTTGTTTGG-3'
SOX2 fw	5'- GGGAAATGGGAGGGGTGCAAAAGAGG-3'
SOX2 rev	5'-TTGCGTGAGTGTGGATGGGATTGGTG-3
OCT 3/4 fw	5'-GACAGGGGGAGGGGAGGAGCTAGG-3'
OCT 3/4 rev	5'-CTTCCCTCCAACCAGTTGCCCCAAAC-3'
Nanog fw	5'-TGCAAGAACTCTCCAACATCCT-3'
Nanog rev	5'-ATTGCTATTCTTCGGCCAGTT-3'
PDX1 fw	5'-AAGCTCACGCGTGGAAAG-3'
PDX1 rev	5'-GGCCGTGAGATGTACTTGTTG-3'
SOX7 fw	5'-TGAACGCCTTCATGGTTTG-3'
SOX7 rev	5'-AGCGCCTTCCACGACTTT-3'
AFP fw	5'-GTGCCAAGCTCAGGGTGTAG -3'
AFP rev	5'-CAGCCTCAAGTTGTTCCTCTG-3'
CD31 fw	5'-ATGCCGTGGAAAGCAGATAC-3'
CD31 rev	5'-CTGTTCTTCTCGGAACATGGA-3'
Acta-2 fw	5'-GTGATCACCATCGGAAATGAA-3'
Acta-2 rev	5'-TCATGATGCTGTTGTAGGTGGT-3'
SCL fw	5'-CCAACAATCGAGTGAAGAGGA-3'
SCL rev	5'-CCGGCTGTTGGTGAAGATAC-3'
CDH5 fw	5'-GAGCATCCAGGCAGTGGTAG-3'
CDH5 rev	5'-CAGGAAGATGAGCAGGGTGA-3'
KRT14 fw	5'-CACCTCTCCTCCTCCCAGTT-3'
KRT14 rev	5'-ATGACCTTGGTGCGGATTT-3'
NCAM1 fw	5'-CAGATGGGAGAGGATGGAAA-3'
NCAM1 rev	5'-CAGACGGGAGCCTGATCTCT-3'
TH fw	5'-TGTACTGGTTCACGGTGGAGT-3'
TH rev	5'-TCTCAGGCTCCTCAGACAGG-3'
Gabbr-2 fw	5'-CTGTGCCTGCCAGAGTTTCA-3'
Gabbr-2 rev	5'-ACGGCCTTGACGTAGGAGA-3'
GATA4 fw	5'-AGCCTGGCCTGTCATCTCACT-3'
GATA4 rev	5'-GGCCAGACATCGACTAGACT-3'
Mef2c fw	5'-ATCGTTGTTGCCGTCGTTTT-3'
Mef2c rev	5'-CGGCTTCGGTGTCCTCTCT-3'
Tbx5 fw	5'-GACCATCCCTATAAGAAGCCCT-3'
Tbx5 rev	5'-TGTGCCGACTCTGTCCTGTA-3'

(Cond..)

Table 2. *(Continued...)*

Primer	Sequence
Nkx2.5 fw	5'-ACCCAGCCAAGGACCCTAGA-3'
Nkx2.5 rev	5'-CAGCTCCAAAGCCTTCTG-3'
MYLC2a fw	5'-CTTGTAGTCGATGTTCCCCG-3'
MYLC2a rev	5'-TCAAGCAGCTTCTCCTGACC-3'
alpha-Sarc fw	5'-TGTCCTGAGACACTCTTC-3'
alpha-Sarc rev	5'-TGATGCTATTGTAAGTTGTT-3'
alpha-MHC fw	5'-GACTGTTGTGGCCCTGTACCA-3'
alpha-MHC rev	5'-GACACCGTCTGGAAGGATGAG-3'
beta-MHC fw	5'-GATTATGCATTCATCTCC-3'
beta-MHC rev	5'-AGCTTATACATGGAGTTTTT-3'
HCN1 fw	5'-TGAAGCTGACAGATGGCTCTT-3'
HCN1 rev	5'-CTGGCAGTACGACGTCCTTT-3'
HCN2 fw	5'-CTGATCCGCTACATCCATCA-3'
HCN2 rev	5'-AGATTGCAGATCCTCATCACC-3'
HCN3 fw	5'-TGGATCCTACTTTGGGGAGA-3'
HCN3 rev	5'-ATGGTCCACGCTGAGTGAGT-3'
HCN4 fw	5'-AACAGGAGAGGGTCAAGTCG-3'
HCN4 rev	5'-ATCAGGTTTCCCACCATCAG-3'
CACNA1C fw	5'-CCTGCTGACTCCCAGAAGAC-3'
CACNA1C rev	5'-AGAGGCACAGAGGGAGTCAA-3'
CACNA1G fw	5'-GAACCGTCCTGCTCTCTAGC-3'
CACNA1G rev	5'-GGGCTGCATATTGCTCTCCA-3'
EBNA-1 fw	5'-ATCAGGGCCAAGACATAGAGATG-3'
EBNA-1 rev	5'-GCCAATGCAACTTGGACGTT-3'
FBOX-15 fw	5'-GCCAGGAGGTCTTCGCTGTA-3'
FBOX-15 fw	5'-AATGCACGGCTAGGGTCAAA-3'
GAPDH fw	5'-CCACCCATGGCAAATTCC-3'
GAPDH rev	5'-TCGCTCCTGGAAGATGGTG-3'

3.13. MicroRNA profiling

Comparative microRNA (miR) expression profiling was carried out using TaqMan Low Density Arrays for the Human MicroRNA A and B Card Sets v3.0 (Applied Biosystems), according to the manufacturer's instructions, using a 7900TH Real-Time PCR System (Applied Biosystems). Prior to the analysis, probes were renamed and reannotated according to miRBase Release 20 (http://www.mirbase.org) (23). This allowed us to identify target sequences unique to human miRs, discarding probes for tRNAs, snoRNAs, and misannotated sequences. Quality control analysis and relative quantitation of data generated with TaqMan Arrays were performed using the SDS RQ Manager Software v1.2.1 and the DataAssist Software v3.01

Table 3. Immunophenotyping of fetal *vs* adult SStCs and CStCs

Marker	Fetal SStCs (%)	Adult SStCs (%)	Fetal CStCs (%)	Adult CStCs (%)
CD 13	98.4±0.4	99.2±0.8	74.1±23.5	98.9±0.6
CD 29	98.3±0.4	95.9±3.0	97.8±1.2	98.3±0.8
CD 44	97.2±1.3	95.9±2.2	96.5±1.0	97.8±0.8
CD 73	92.7±5.5	90.9±2.3	91.5±6.1	91.2±14.4
CD 90	95.1±5.4$^{\$}$	85.3±15.0$^{\$}$	53.7±34.8*	36.4±16.8
CD 105	78.5±16.9	59.5±29.5	74.8±28.3	89.4±8.4
CD 146	68.1±16.0	46.6±24.8	82.7±8.9§	38.2±26.8
CD 14	0.0±0.0	0.0±0.0	0.0±0.0	0.0±0.0
CD 31	1.0±2.0	0.2±0.4	3.2±3.7	2.2±2.5
CD 34	0.0±0.0	0.0±0.0	0.0±0.0	0.0±0.0
CD 45	0.0±0.0	0.0±0.0	0.0±0.0	0.0±0.0
CD 144	0.0±0.0	0.0±0.0	6.9±8.0	4.6±7.8
VEGFR2	2.2±1.1	0.5±0.9	2.4±1.9	1.4±0.8
C-KIT	3.4±4.8	1.4±1.2	2.4±2.3	1.8±1.1
HLA-DR	0.0±0.0	0.0±0.0	0.0±0.0	0.0±0.0
HLA-ABC	93.0±1.0	79.7±8.9	90.0±4.3	85.0±0.9
Chondroitin sulfate	99.1±0.4	91.8±9.1	88.7±17.4	71.4±14.8
Nestin	89.1±9.6	86.4±7.3	83.7±11.4	89.4±4.9

One-way ANOVA followed by Bonferroni's test for multiple comparison, *p<0.05 *vs* fetal SStCs, $^{\$}$p<0.001 *vs* adult CStCs, §p<0.05 *vs* adult CStCs

(Applied Biosystems). All Ct values reported as greater than 40 or as not detected were changed to 40 and considered a negative call. Raw expression intensities of target miRs were normalized for differences in the amount of total RNA added to each reaction using the mean expression value of all expressed miRs in a given sample (24). Relative quantitation of miR expression was performed using the comparative Ct method (ΔΔCt). MiRs were deemed as non-informative and filtered out when the percentile of negative calls exceeded 4 (25 percent of the samples).

3.14. MicroRNA profiling data analysis

Differential expression analysis was performed using the module LIMMA (Linear Models for Microarray Data) implemented in the Multi Experiment Viewer (MeV) software package v4.9.0 (25, 26). Data were $\log_2$ transformed and the two-factor design (tissue and cell type) option was chosen. LIMMA performed the moderated t-statistic for each miR and for each contrast, using an empirical Bayes shrinkage method to borrow information across genes, making the inference about each individual miR stable even for experiments with a small number of arrays. P-values were calculated adjusting for multiple testing using the Benjamini and Hochberg's method to control the false discovery rate (FDR). Adjusted p-values less than 0.05 were considered statistically significant. Unsupervised hierarchical clustering analyses of samples and miRs were performed on $\log_2$-transformed, mean-centered values by Pearson's centered correlation as distance metric and average linkage method, with leaf ordering optimization, using the module implemented in MeV. Experimentally validated miR-target interactions were derived from the databases DNA Intelligent Analysis (DIANA) TarBase v6.0 and miRTarBase Release 4.5 (27, 28). Functional annotation analysis on validated targets of the differentially expressed miRs was carried out using either the DNA Intelligent Analysis (DIANA) miRPath v2.0 or the Database for Annotation, Visualization and Integrated Discovery (DAVID) v6.7 (29, 30). DIANA miRPath was used to perform gene-enrichment analysis in KEGG pathways; DAVID was used for Gene Ontology (GO) terms (Biological Process and Molecular Function categories). Over-representation statistical analysis was performed by conservative adjustments of Fisher's exact test, followed by Benjamini and Hochberg's correction for FDR. Statistical significance level was set for adjusted p-values less than 0.05. Redundant GO terms were removed using the web-based tool Reduce and Visualize Gene Ontology (REViGO), with an allowed similarity threshold of 0.5 (31).

3.15. Statistical analysis

Data were presented as mean ± SD. Statistical analysis was performed using ANOVA or Student *t*-test when appropriate (see figure/table captions for the test used for each specific experiment). A p-value less than 0.05 was considered statistically significant.

4. RESULTS

4.1. Morphology, immunophenotyping and cardiomyogenic potential of skin and cardiac fetal stromal cells

Fetal stromal cells were isolated as heterogeneous populations from cardiac (CStC) and skin (SStC) fibroblasts of the same aborted fetus of pregnant women between 12th -16th week of gestation (n=4 pairs of stromal cells). CStCs and SStCs cultured in GM presented a fibroblast-like morphology, indistinguishable from that of adult stromal cells obtained from skin and right auricle (Figure 1A). Both CStCs and SStCs expressed immunophenotypic markers associated with mesenchymal stromal cells, *i.e.* CD13, CD29, CD44, CD73, and CD105, and were negative for the expression of CD14, CD34, CD45, and HLA-DR (Figure 1B and Table 3). As previously described, CD90 showed a variable expression in the different stromal cell populations and was generally higher in both fetal and adult SStCs than CStCs (Table 3) (14, 32). A higher number of CStCs were positive for CD146 compared to

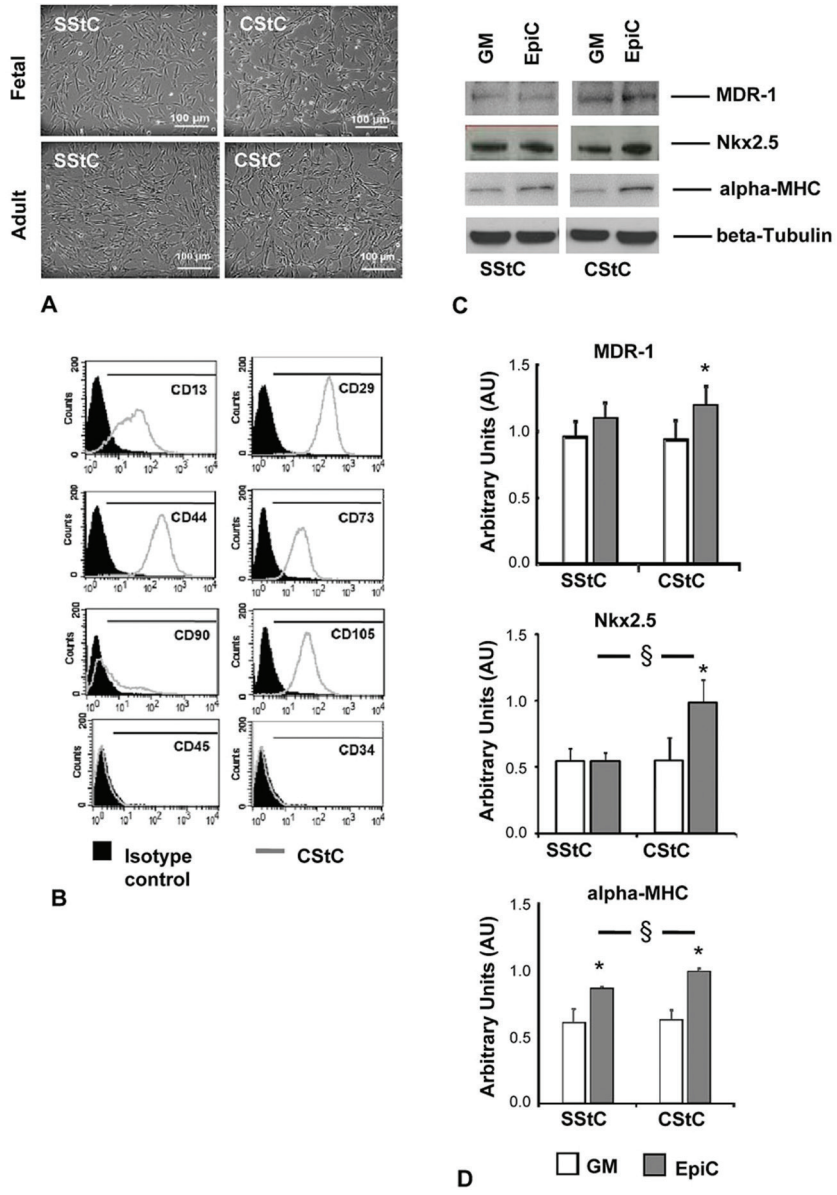

Figure 1. Morphology, immunophenotyping and cardiac potential. A) SStCs and CStCs expanded in GM showed a fibroblast-like shape, indistinguishable from stromal cells obtained from adult skin and right auricle (cardiac origin). Original magnification 10 x; scale bar 100 µm. B) Representative FACS cytograms of CStC surface marker expression. C) Representative immunoblot showing expression in SStCs and CStCs of cardiac precursor markers MDR-1 (170 kDa), Nkx2.5 (40 kDa), and alpha-MHC (200 kDa) in GM and after EpiC treatment. D) Densitometry for each marker is represented in the bar graphs as average results, normalized to beta-tubulin (50 kDa) (n=4, Student t-test: *p<0.05 vs GM, §p<0.01 *vs* SStCs in EpiC). SStCs = fetal skin stromal cells, CStCs = fetal cardiac stromal cells, GM = growth medium, EpiC = Epigenetic cocktail medium.

SStCs (Table 3), indicating that a greater proportion of perycytes is present in the fetal cardiac population (33). We evaluated the ability of CStCs *vs* SStCs to express cardiomyocyte lineage markers by performing an *in vitro* assay as previously reported (15). Specifically, culturing CStCs for 7 days in cardiogenic medium (EpiC medium) significantly increased the protein levels of the cardiac progenitor marker MDR-1, the cardiac mesoderm marker Nkx2.5, and the cardiomyocyte sarcomeric protein alpha-MHC when compared to CStCs expanded in GM (Figure 1C-D) (15, 16, 34). In contrast, the same treatment of SStCs only, led to a significant increase in alpha-MHC protein (Figure 1C-D). Of note, alpha-MHC expression was significantly higher in Epic-treated CStCs compared to Epic-treated SStCs.

4.2. Characterization of iPSCs derived from CStCs *vs* SStCs

We generated and tested for successful pluripotent reprogramming of iPSC clones from each

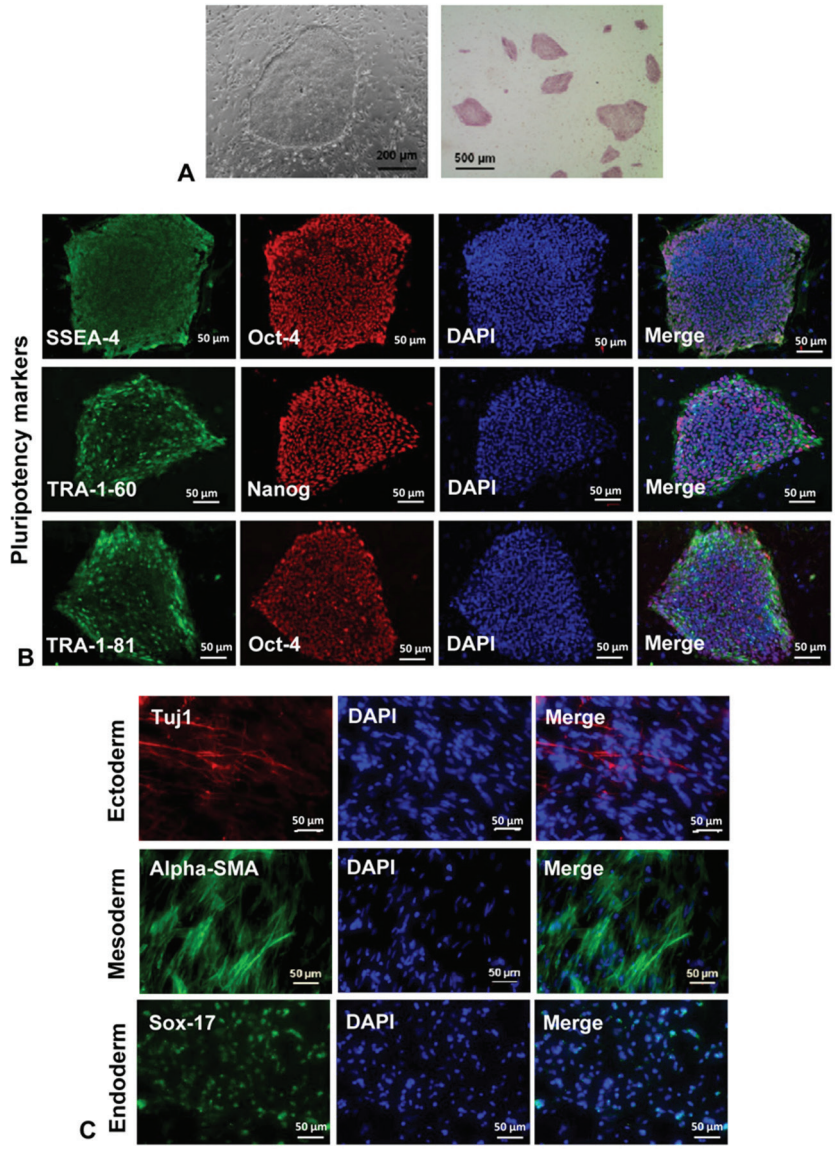

Figure 2. Characterization of iPSCs obtained from CStCs. A) Colonies of CStC-derived iPSCs showing a typical embryonic-stem cell morphology. Original magnification 10 x; scale bar 200 µm (on the left). Representative examples showing the positive staining for alkaline phosphatase in C-iPSCs. Positive colonies appear pink. Original magnification 4 x; scale bar 500 µm (on the right). B) Immunofluorescence analysis for expression of the pluripotency proteins SSEA-4, TRA-1-60, TRA-1-81, Oct-4 and Nanog in C-iPSCs. Original magnification 20 x; scale bar 50 µm. C) Differentiated embryoid bodies (EBs) in C-iPSCs stained positive for three germ layer markers: Tuj1 as a marker for neural progenitor cells (ectoderm), alpha-smooth muscle actin (mesoderm) and Sox17 for endodermal progenitor cells (endoderm). Original magnification 20 x; scale bar 50 µm. All the results represented in this Figure were comparable to those obtained in iPSCs from SStCs. iPSCs= induced pluripotent stem cells, S-iPSCs= iPSCs obtained from SStCs, C-iPSCs= iPSCs obtained from CStCs.

CStCs and SStCs of the same individual. Three unrelated aborted fetuses were used to create three pairs of skin and cardiac iPSCs. The efficiency of reprogramming (0.002-0.005 percent of transfected cells) is comparable in both SStCs and CStCs. All iPSC clones showed human embryonic stem cell-like morphology and were highly positive for alkaline phosphatase staining (Figure 2A). RT-qPCR analysis revealed that all iPSC clones expressed endogenous pluripotency genes (SOX2, OCT3/4, Nanog) at significantly higher levels than parental fetal stromal cells (Table 4). Importantly, all iPSC lines showed no expression of exogenous episomal transgenes, thus confirming successful activation of endogenous pluripotency genes without genome-integration of exogenous vectors (not shown). Finally, each line expressed the pluripotency markers Oct-4, Nanog, SSEA-4, Tra 1-60, and Tra 1-81 at the protein level (Figure 2B). All iPSC clones were able to form embryoid bodies (EBs) and differentiate into cells of the three germ layers, staining positive for ectodermal (Tuj1),

Table 4. Fold variation in mRNA expression (mean±SD) of pluripotency genes in StCs *vs* iPSCs

Genes	SStCs	S-iPSCs	CStCs	C-iPSCs
c-MYC	1.09±0.56	1.01±0.40	1.40±1.43	0.38±0.12
KLF4	1.39±1.34	1.16±0.51	1.32±0.93	0.62±0.17
SOX2	1.03±0.34	19931.23±7430.70**	2.43±3.52	3195.70±1032.74*
OCT3/4	1.43±1.03	1081.92±258.56*	1.08±0.56	513.41±125.14**
Nanog	1.12±0.55	1083.45±87.44**	1.44±1.29	2346.23±660.69**

SStCs: Fetal skin stromal cells; CStCs: Fetal cardiac stromal cells; S-iPSCs: iPSCs obtained from SStCs; C-iPSCs: iPSCs obtained from CStCs. Student *t*-test (n=3), *p<0.05 and **p<0.01 *vs* corresponding primary fetal fibroblasts

Table 5. Fold variation in mRNA expression (mean±SD) of three germ layer genes in iPSCs *vs* EBs at 15-20 days of differentiation

Genes	S-iPSCs	S-iPSC-EBs	C-iPSCs	C-iPSC-EBs
PDX1 (end)	1.02±0.22	7.22±5.42*	1.14±0.73	10.49±0.89**
SOX7 (end)	1.09±0.46	4.45±3.02*	1.41±1.30	3.80±4.11
AFP (end)	1.08±0.41	61.59±31.68**	1.12±0.58	289.72±96.95*
CD31 (mes)	1.30±0.88	20.79±7.33**	1.13±0.57	11.35±0.84**
Acta-2 (mes)	1.33±1.30	17.43±7.42**	1.89±2.15	35.26±21.48*
SCL (mes)	1.38±0.83	3.98±1.43*	2.47±2.89	11.65±13.82
CDH5 (mes)	1.05±0.41	6.03±1.87**	2.53±2.78	24.63±14.86*
KRT14 (ect)	1.23±0.71	54.28±25.35**	1.96±2.71	36.75±25.49*
NCAM1 (ect)	1.04±0.33	6.95±1.78**	2.08±2.69	18.50±10.77*
TH (ect)	1.15±0.65	4.56±2.92**	1.75±1.95	14.11±8.78*
Gabbr-2 (ect)	1.11±0.50	28.00±19.06*	2.14±2.10	19.83±12.84*

S-iPSCs: iPSCs obtained from SStCs; C-iPSCs: iPSCs obtained from CStCs; S-iPSC-EBs: Embryoid bodies obtained from S-iPSCs; C-iPSC-EBs: Embryoid bodies obtained from C-iPSCs; end: Endoderm; mes: Mesoderm; ect: Ectoderm. Student t-test (n=3), *p<0.05 and **p<0.01 *vs* corresponding iPSC counterpart

mesodermal (alpha-SMA) and endodermal (Sox-17) markers, respectively (Figure 2C). In addition, most of the endoderm (PDX1, SOX7, and AFP), mesoderm (CD31, ACTA2, SCL, and CDH5) and ectoderm (KTR14, NCAM1, TH, and GABRR2) genes analyzed had significantly up-regulated expression in EBs at day 15-20 of differentiation when compared to undifferentiated iPSCs (Table 5) (18).

4.3. Efficiency of cardiac differentiation of C-iPSCs *vs* S-iPSCs

IPSC clones derived from three matching pairs of CStCs and SStCs were differentiated into beating EBs using cardiogenic medium (18, 19). Spontaneous beating foci started to appear 10 days after starting differentiation for both S-iPSCs and C-iPSCs, and their number gradually increased until reaching a plateau around 18-20 days into differentiation. The number of beating EBs was significantly higher in cultures of C-iPSCs in comparison with S-iPSCs (Figure 3A). Also, FACS analysis showed a significant increase in Troponin T (Tn-T) positive cells within EBs obtained from C-iPSCs compared to S-iPSCs (Figure 3B). Beating areas were then dissected from beating clusters at day 20-25, to obtain cardiomyocyte-enriched preparations for subsequent characterization. Manually dissected beating areas (Beaters) had a diameter ranging from 200 to 500 µm. The dimensions of beating clusters were not significantly different between beating EBs from S-iPSCs and C-iPSCs (not shown). FACS analysis revealed that dissected beating areas are enriched in Tn-T positive cells compared to parental EBs and specifically, that the number of Tn-T positive cells was higher in C-iPSCs dissected beaters compared to S-iPSCs (Figure 3B). Both S-Beaters and C-Beaters expressed cardiac specific Troponin I (Tn-I) and alpha-Actinin organized in a sarcomeric pattern (Figure 3C). Further, RT-qPCR analysis showed that the expression levels of early cardiac mesoderm markers (GATA4, Mef2c and Tbx5) were similar between S- and C-Beaters after 30 days of differentiation (Figure 4A), while C-Beaters expressed significantly higher Nkx2.5 and cardiomyocyte markers (MYLC2a, alpha-Sarc, alpha-MHC, and beta-MHC) levels than S-Beaters (Figure 4B). Additionally, C-Beaters exhibited higher expression than S-Beaters of a specific subset of cardiac ionic channels, namely HCN1, HCN2, HCN4 (responsible for pacemaker channels), CACNA1C and CACNA1G (the alpha-subunits for L-type and T-type calcium channels, respectively) (Figure 5A). The expression of HCN3 did not differ between the two populations (Figure 8A). Finally, the expression levels of myomiRs (miR-1, -133a, and -133b) are significantly higher in C-Beaters than S-Beaters, while miR-208a did not significantly differ between beaters from the two populations (Figure 5B).

4.4. Functional characteristics of dissected beaters

Figure 6 shows the electrophysiological properties of S-Beaters and C-Beaters. Action potentials of whole beating areas derived from either S-iPSCs or

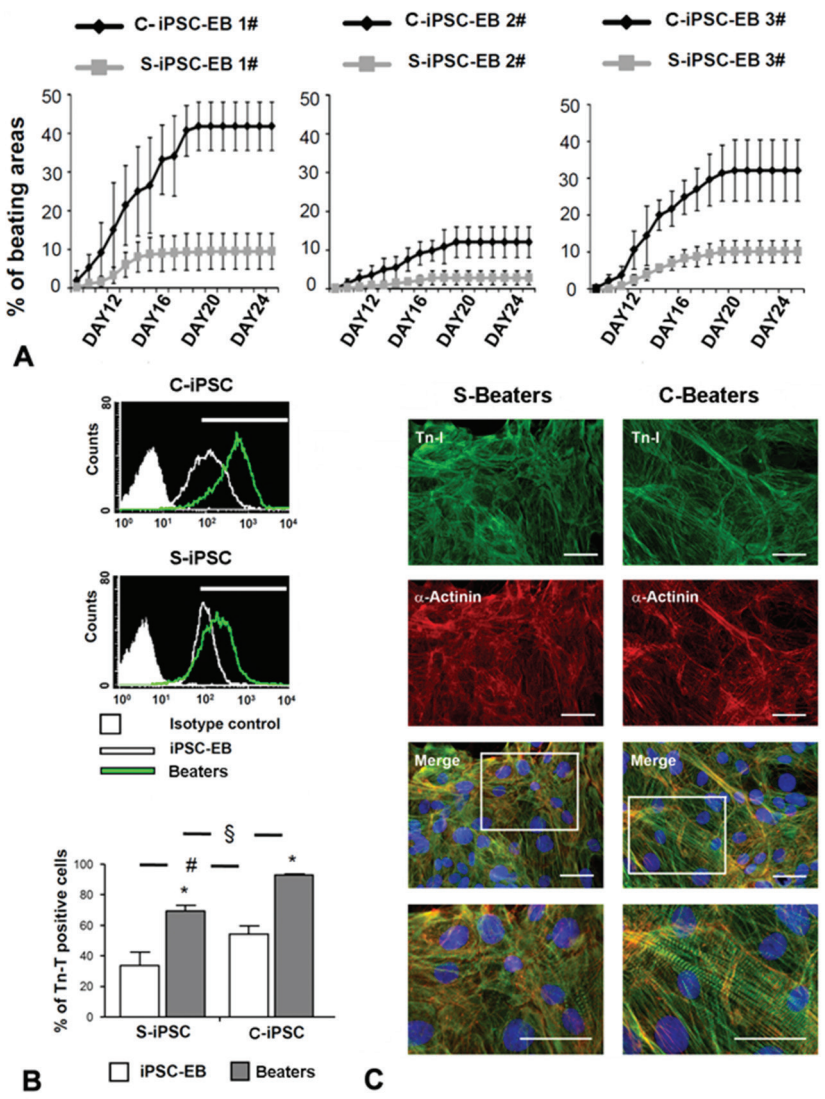

Figure 3. Characterization of cardiomyocytes derived from C-iPSCs and S-iPSCs. A) Curves indicating the increasing number of spontaneous beating foci in both C-iPSC-EBs and S-iPSC-EBs between days 9-25 of differentiation. Each line graph shows the results obtained from each donor (#1, #2 and #3), reporting the average values of a minimum of 4 independent differentiation experiments. The number of beating areas was significantly higher in C-iPSCs compared to S-iPSCs at all times (Repeated measures two-way ANOVA, $p<0.001$). B) Representative FACS cytograms of Tn-T expression in iPSC-EBs and Beaters manually dissected obtained from S-iPSCs and C-iPSCs from each donor and bar graph indicating average results of Tn-T positive cells, evaluated by FACS analysis (n=3; Student t-test :*$p<0.01$ *vs* corresponding iPSC-EB counterpart, #$p<0.05$ *vs* S-iPSC-EBs, $^{§}p<0.001$ *vs* S-Beaters). C) Representative pictures of immunofluorescence staining for cardiomyocyte sarcomeric proteins Troponin I (Tn-I) and alpha-Actinin performed on dissected beating areas obtained from S-iPSCs and C-iPSCs at day 60 of differentiation. Nuclei are counterstained in blue (DAPI). In the bottom panels, magnifications of the framed areas are reported, displaying clear and organized sarcomere structures. Original magnification 40 x; scale bar 25 µm. iPSC-EBs = Embryoid bodies obtained from iPSC differentiation.

C-iPSCs were recorded with the patch-clamp technique in whole-cell-current-clamp mode for functional analysis after 30 days or 60 days of differentiation (Figure 6A). The beating rates were similar regardless of the age or the origin of beating clusters (Figure 6A; see Table 6 for detailed values). In contrast, 60 day-old C-Beaters displayed significantly more hyperpolarized maximum diastolic potentials (MDPs) and higher action potential (AP) amplitudes when compared to either 30 day-old C-Beaters or 60 day-old S-Beaters (Figure 6B-C and Table 6). These data may suggest a higher degree of electrical maturation of C-Beaters with respect to S-Beaters. S-Beaters demonstrated limited electrical maturation from 30 to 60 days of differentiation in standard cardiogenic medium (Figure 6B-C). Furthermore, compared to 30 day-old C-Beaters, 60 day-old C-Beaters showed less increase in beating rate when challenged with a saturating concentration (1 microM) of isoproterenol (Figure 6D-E), indicating potential maturation toward working cardiomyocytes

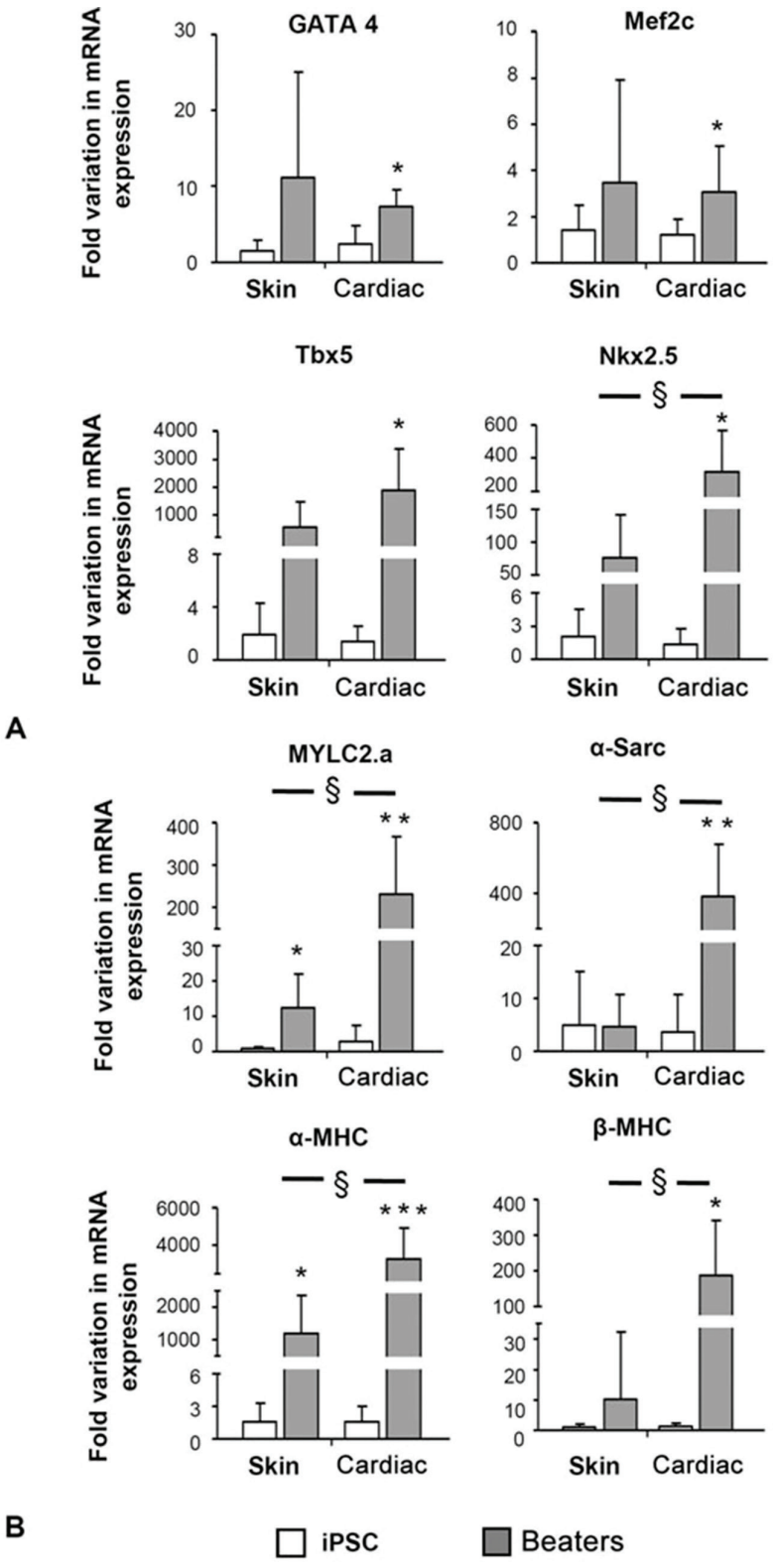

Figure 4. Expression analysis for cardiac genes in cardiomyocytes obtained from C-iPSCs *vs* S-iPSCs. RT-qPCR analysis of A) early cardiac markers GATA4, Mef2c, Tbx5 and Nkx2.5 and B) late cardiac markers Myosin Light Chain 2a (MYLC2a), alpha-Sarcomeric Actin (alpha-Sarc), alpha- and beta-Myosin Heavy Chain (alpha-MHC, beta-MHC) in C-Beaters and S-Beaters after 30 days of differentiation (n=3, unpaired Student *t*-test: *p<0.05, **p<0.01, ***p<0.001 *vs* corresponding undifferentiated iPSC counterpart, §p<0.05 *vs* S-Beaters).

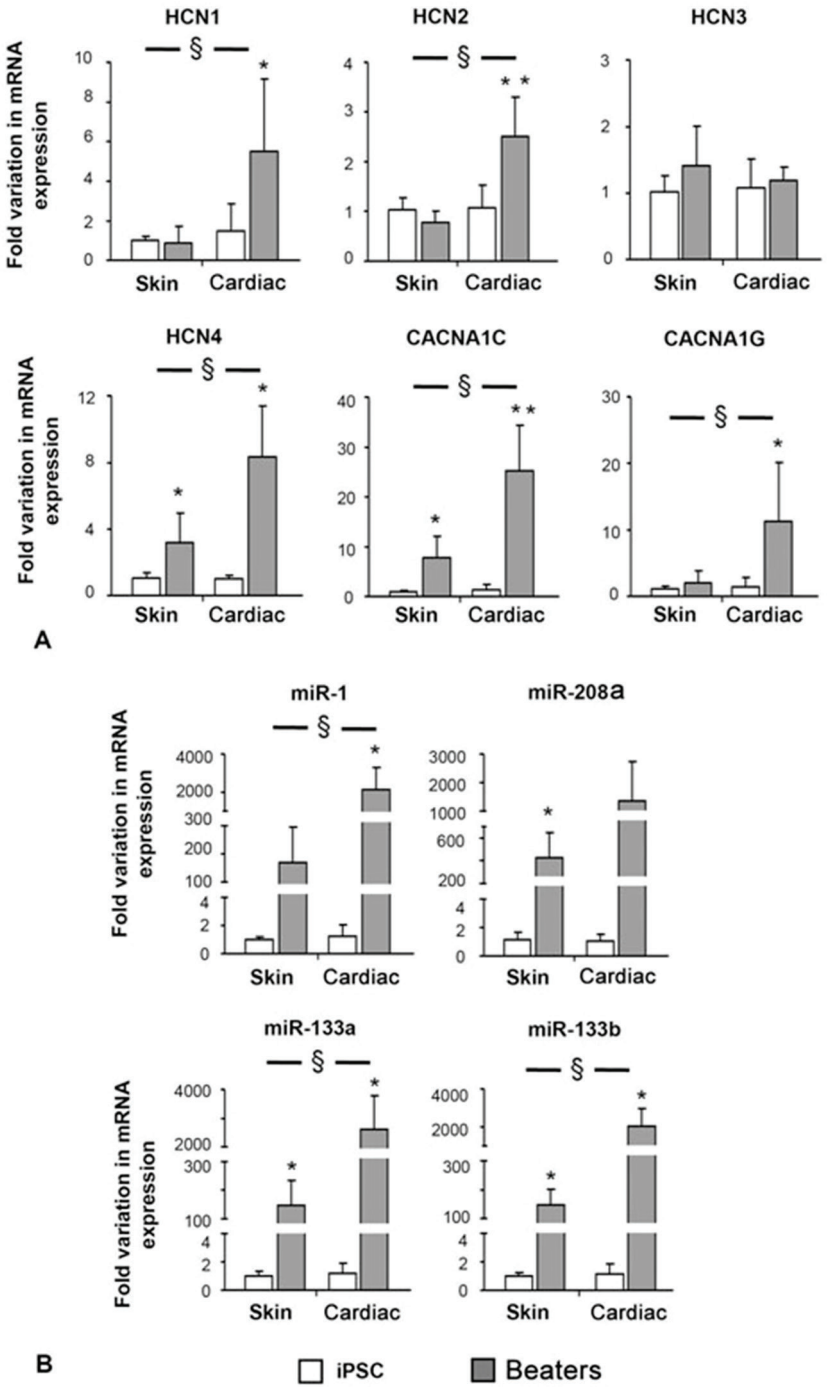

Figure 5. Expression of ion-channel markers and myomiRs in C-Beaters *vs* S-Beaters. RT-qPCR analysis for A) ion-channel markers HCN1, HCN2, HCN4, HCN3, CACNA1C and CACNA1G in C-Beaters and S-Beaters at day 30 of differentiation. B) qRT-PCR analysis of typical myomiR expression (miR-1, -208, -133a, -133b) in C-Beaters and S-Beaters after 30 days of differentiation (n=3, unpaired Student *t*-test: *p<0.05, **p<0.01, ***p<0.001 *vs* corresponding undifferentiated iPSC counterpart, §p<0.05 *vs* S-Beaters).

with less adrenergic response in their automaticity. Of note, evaluating both kinematics and dynamics revealed that C-Beaters after 20-25 days of differentiation were characterized by significantly higher contractility than S-Beaters (Figure 6F), whereas, in agreement with patch-clamp recordings, no significant difference was found in terms of contraction frequency (data not shown).

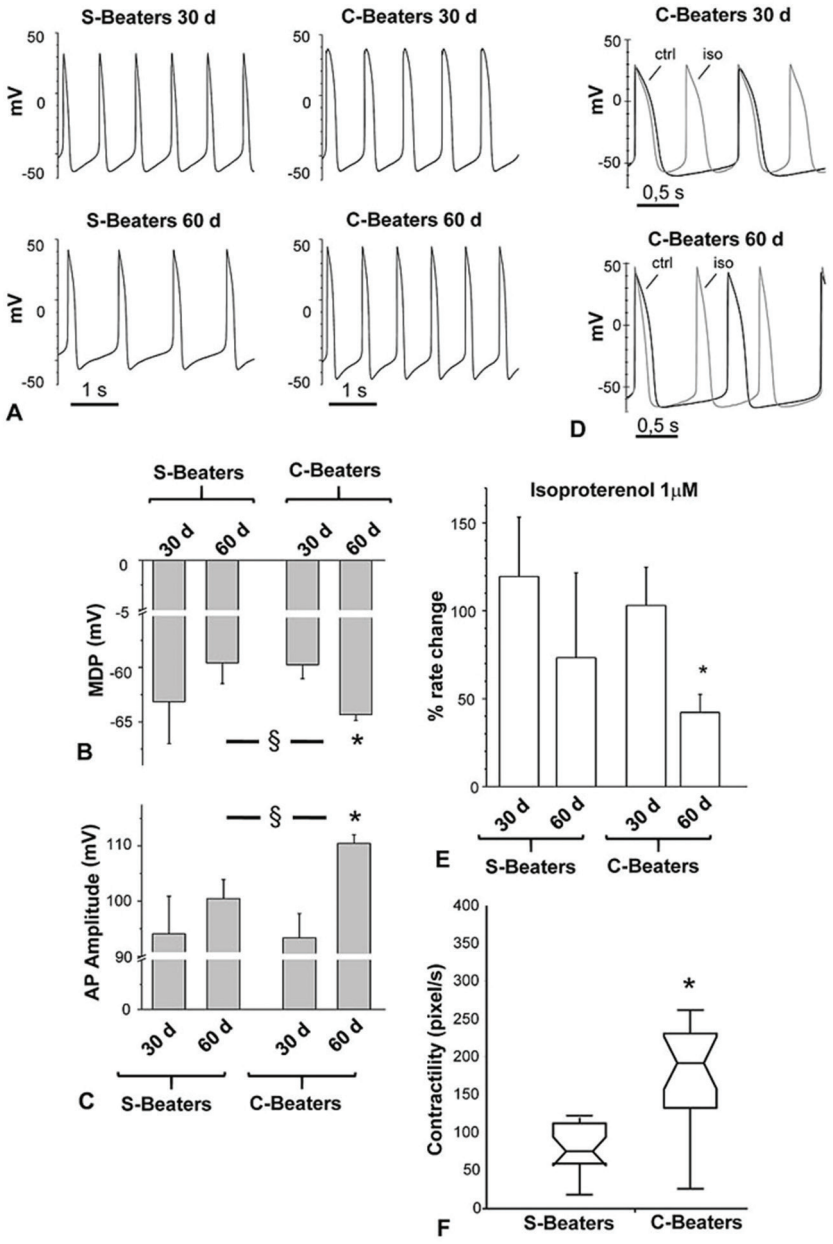

Figure 6. Functional characteristics of C-Beaters vs S-Beaters. A) Examples of spontaneous action potentials recorded in C-Beaters and S-Beaters after 30 or 60 days of differentiation. Bar graphs indicating B) the maximum diastolic potential (MDP) and C) amplitude of beating portions derived from 30 or 60 day-old C-Beaters *vs* S-Beaters. D) Representative action potential recordings of 30 or 60 day-old C-Beaters before and after exposure to a saturating concentration (1 microM) of isoproterenol. E) Bar graphs showing the percentage of spontaneous firing rate change normalized to control rate of 30 or 60 day-old S-Beaters and C-Beaters before and after the exposure to isoproterenol (1 microM). (Unpaired Student's test was used to compare groups. S-Beaters 30 days n=3, S-Beaters 60 days n=5, C-Beaters 30 days n=13, C-Beaters 60 days n=16. *p<0.05 *vs* 30 days, §p<0.05 *vs* S-Beaters). F) Graphs showing contractility (p-value = 0.0005) in C-Beaters and S-Beaters after 20-25 days of differentiation (S-Beaters n=10, C-Beaters n=12; Kruskal-Wallis test, followed by Dunn-Sidák correction).

4.5. miR profiling of CStCs *vs* SStCs and their iPSC counterpart

Potential involvement of miRs in affecting iPSC differentiation was assessed by miR expression profiling on CStCs, SStCs and their iPSC counterparts. After applying quality and filtering criteria, 482 miRs were considered for subsequent analyses. An unsupervised hierarchical clustering analysis, performed on the entire miR profiles of both cardiac and skin stromal cells before and after the reprogramming process, showed that cells clustered together in relation to their state (founder

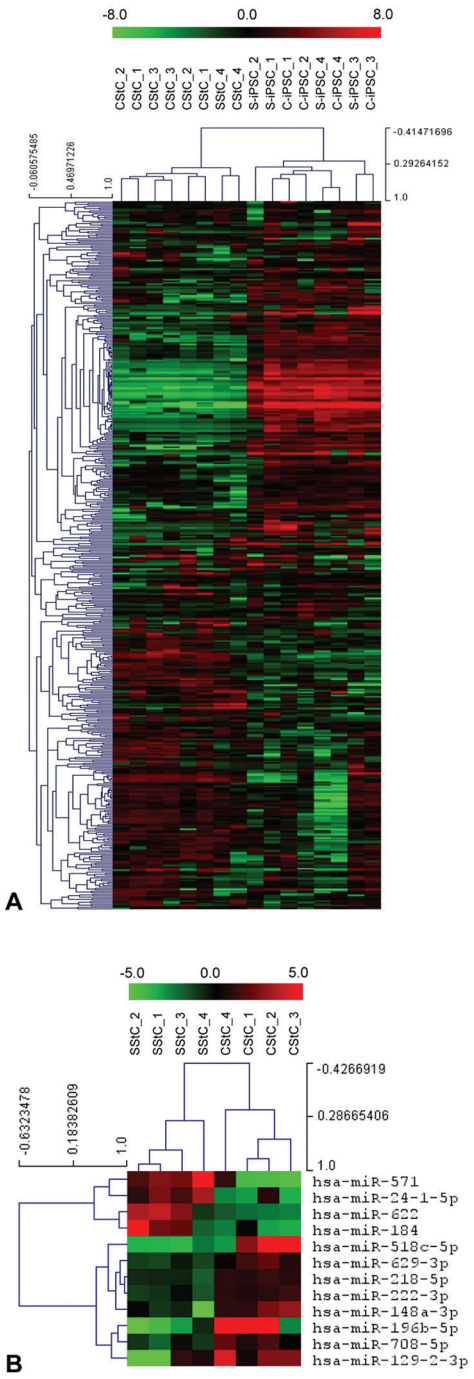

Figure 7. Hierarchical clustering of miRs expressed in StCs *vs* iPSCs from cardiac and skin origins. A) Unsupervised analysis was performed using the whole dataset of miRs that passed the quality assurance and filtering criteria: the global expression profile clearly discriminates StCs from their iPSC counterpart after induction of pluripotency, irrespective of the tissue of origin. The mean centered value of normalized $\log_2$ transformed relative expression level of each miR is represented with a green, black, and red color scale (green indicates below mean; black, equal to mean; and red, above mean). B) Unsupervised hierarchical clustering of miRs differentially expressed in CStCs *vs* SStCs before and after reprogramming. Heatmap showing the 12 miRs differentially expressed between CStCs and SStCs (8 miRs overexpressed and 4 decreased in CStCs).

vs reprogrammed) and/or source fetus, independently of the tissue origin (Figure 7A). This observation suggests that the reprogramming process resulted in extensive modifications of cellular miR expression and likely diminished tissue-specific differences. This is confirmed by the LIMMA analysis, which revealed that 12 miRs appeared differentially expressed between CStCs and SStCs (4 overexpressed and 8 decreased, respectively) at a nominal p-value less than 0.01 (Figure 7B), but this difference did not withstand correction for multiple comparisons. This probably reflects a high inter-individual variability in miR expression. Most importantly, these differences in the miR expression profiles between the founder stromal cells was lost after induction of pluripotency, as these miRs did not show any significant differential expression between the iPSC counterparts (Table 7). Of note, only 2 miRs were overexpressed in C-iPSCs *vs* S-iPSCs, at a nominal p-value less than 0.01, but again this did not withstand FDR correction (Table 7). The impact of reprogramming on miR expression was further elucidated when we compared fetal stromal cells derived from heart or skin with their reprogrammed iPSC counterpart. LIMMA analysis allowed us to identify 167 miRs significantly modulated by the induction of pluripotency, with a FDR-adjusted p-value less than 0.05. Most of these miRs were similarly modulated in cells both of cardiac and skin origin. Of note, 33 miRs were specifically modulated in cardiac cells, whereas 43 were exclusive for skin cells (Figure 8 and Table 8). Gene-enrichment analysis in KEGG pathways (Table 9), conducted on validated targets of miRs specifically modulated by reprogramming process in the two cell types, revealed that these miRs may interact both with common (*i.e.* Akt, p53, cell cycle) and distinct pathways (*i.e.* VEGF and TGF-beta signaling for cardiac cells, HIF-1 signaling in skin cells). Finally, we performed a gene-enrichment analysis in GO terms for Biological Processes and Molecular Function on validated miR-target interactions, excluding those categories significantly enriched in both cell types after reprogramming. This analysis revealed that miRs modulated in cells of cardiac origin may interact with ribosome biogenesis and metabolism and mRNA stability, ER-nuclear signaling pathways, and cell morphogenesis and differentiation (Table 9). Interestingly, miRs predicted to target histone deacetylase (HDAC) binding were modulated by the reprogramming process only in cells of atrial origin (Table 9). Following this line of evidence, we performed Western Blot analysis on two putative target proteins belonging to HDAC binding class, GCN5 and P300/CBP-associated factor (PCAF). Of note, GCN5 protein level was significantly lower in C-iPSCs than in S-iPSCs, whereas PCAF protein level remained unchanged (data not shown). Conversely, our analysis revealed that miRs differentially expressed in skin may target genes involved in cell

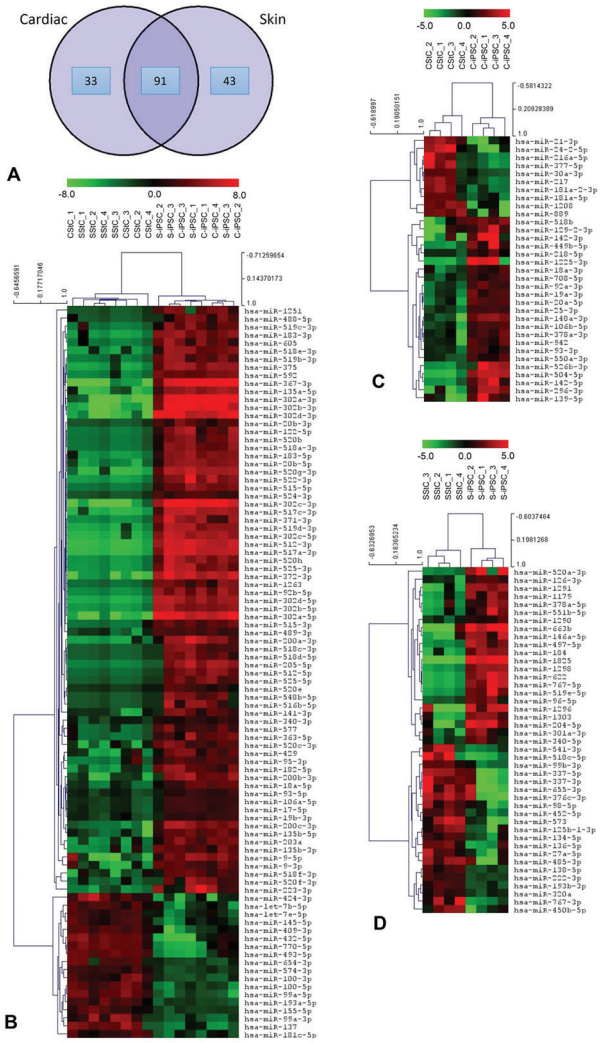

Figure 8. Heatmaps and clustering analysis of miRs differentially expressed between iPSCs and fetal stromal cells of cardiac and/or skin origin. A) A Venn diagram shows those miRs specifically modulated by the induction of pluripotency in cardiac- (33 miRs) and skin-derived (43 miRs) cells and those similarly modulated in cells both of cardiac and skin origin (91 miRs) (at a FDR-adjusted significance level p<0.0µ5). B) Unsupervised hierarchical clustering showed that the expression profile of these latter 91 miRs completely discriminated stromal cells from iPSCs, irrespective of their tissue of origin. The dendrogram on the left shows two distinct clusters of 73 miRs up- and 18 down-regulated in iPSCs *vs* stromal cells (respectively at the top and the bottom of the heatmap). A similar analysis was performed on the C) 33 miRs specifically modulated in CStCs *vs* C-iPSCs and D) 43 miRs exclusively regulated in SStCs *vs* S-iPSCs. The dendrograms above the heatmaps show that the differential expression profiles completely discriminate the stromal cells from their iPSC counterparts. The dendrograms on the left show distinct clusters of 23 miRs up- and 10 down-regulated and of 22 miRs up- and 21 down-regulated in iPSCs *vs* stromal cells, respectively, in cells of cardiac or skin origin. The mean centered value of normalized $\log_2$ transformed relative expression level of each miR is represented with a green, black, and red color scale (green indicates below mean; black, equal to mean; and red, above mean).

migration, actin filament-based process, epithelial tube formation, senescence and leukocyte cell-cell adhesion (Table 9). This might partially account for the lower cardiogenic potentials of the S-iPSCs.

5. DISCUSSION

The issue of epigenetic memory in iPSCs is still controversial. Although it has been demonstrated that in murine iPSC lines epigenetic markers of the tissue of origin are evident at early passages (*i.e.* less than 10), extended passaging (greater than 20-25) of human iPSCs did not increase their resemblance to human embryonic stem cells (5, 35, 36). This could be interpreted as an incomplete resetting of somatic gene expression and/or epigenetic states in iPSCs, thus underlying the role of the donor epigenetic landscape in determining potential iPSC properties. Consistent with this concept, it has been reported that iPSCs derived from human retinal pigmented epithelial cells (RPE) showed a preferential commitment to spontaneously differentiate back to RPE even after extensive passaging despite being able to give rise to cells of three germ-layers (37).

The present study demonstrated that CStC-derived iPSCs at passages greater than 15 retain a higher tendency to generate cardiomyocytes with more mature characteristics than iPSCs obtained from SStCs, supporting for the first time the existence of a functional memory specifically associated with the stromal components of the tissue of origin. The fact that C-Beaters showed a significant enrichment of Tn-T positive cells than S-Beaters, along with the observation that immunofluorescence analysis does not seem to indicate an higher expression of Tn-I and alpha-Actinin in cardiomyocytes obtained from C-iPSCs *vs* S-iPSCs, seem to support the hypothesis that beaters from C-iPSCs might contain a higher number of cardiomyocytes than dissected beaters from S-iPSCs. In addition, electrophysiological results displayed a more hyperpolarized diastolic potentials and larger action potential amplitudes in C-Beaters compared to S-Beaters, consistent with an increased level of *in vitro* maturation of cardiomyocytes composing C-Beaters. Finally, measuring kinematics and dynamics demonstrated a higher contractility of C-Beaters *vs* S-Beaters thus possibly indicating both a higher number and better *in vitro* maturation of cardiomyocytes in beating syncytia from C-iPSCs.

To exclude that the differences observed in cardiomyogenic differentiation between C-iPSCs and S-iPSCs were related to random clonal events and not to actual epigenetic factors, we generated iPSCs from three independent donors. It is recognized that the variability among different clones obtained from the same individual is lower than the variability among lines from different individuals (38). Although intrinsic line-to-line variability in differentiation capacity can complicate the interpretation of comparative studies, we observed a clear increase of cardiomyogenic efficiency in all the lines derived from cardiac tissue compared

Table 6. Summary of electrophysiological results

	Rate (Hz)	MDP (mV)	AP Amplitude (mV)	Rate change in isoproterenol (%)
S-Beaters 30 days	0.98±0.13 (n=3)	−62.9±3.8 (n=3)	93.3±6.7 (n=3)	119.5±33.1 (n=3)
S-Beaters 60 days	1.01±0.41 (n=5)	−59.3±1.9 (n=5)	99.6±3.4 (n=5)	73.3±48.5 (n=3)
C-Beaters 30 days	1.13±0.14 (n=13)	-59.3±1.3 (n=13)	92.8±4.3 (n=13)	103.2±21.7 (n=11)
C-Beaters 60 days	1.13±0.11 (n=16)	−63.9±0.6*§ (n=16)	−109.9±1.5*§ (n=16)	42.2±10.2* (n=14)

MDP: Mean diastolic potential; AP amplitude: Action potential amplitude. *p<0.05 *vs* 30- days, §p<0.05 *vs* S-Beaters

Table 7. Subset of miRs differentially expressed in CStCs *vs* SStCs before and after reprogramming

miRs	CStCs vs SStCs			C-iPSCs vs S-iPSCs		
	P	adjP	logFC	P	adjP	logFC
hsa-miR-571	0.007	0.36	6.16	0.241	1.00	−2.38
hsa-miR-184	0.004	0.35	4.44	0.560	1.00	0.79
hsa-miR-622	0.001	0.25	4.36	0.289	1.00	−1.13
hsa-miR-24-1-5p	0.002	0.25	4.14	0.249	1.00	1.37
hsa-miR-222-3p	0.003	0.25	−1.94	0.456	1.00	0.41
hsa-miR-2185p	0.010	0.42	−1.98	0.672	1.00	0.29
hsa-miR-708-5p	0.010	0.42	−2.16	0.518	1.00	0.49
hsa-miR-629-3p	0.009	0.42	−2.21	0.557	1.00	0.45
hsa-miR-148a-3p	0.007	0.36	−3.66	0.620	1.00	0.59
hsa-miR-129-2-3p	0.005	0.35	−4.84	0.770	1.00	−0.44
hsa-miR-518c-5p	0.002	0.25	−6.61	0.456	1.00	1.32
hsa-miR-196b-5p	0.001	0.25	−7.60	0.705	1.00	0.74
hsa-miR-655-3p	0.897	0.99	0.21	0.010	0.96	4.75
hsa-miR-449b-5p	0.517	0.99	−0.84	0.004	0.96	4.36

P: p-values; adjP: Benjamini and Hochberg adjusted p-values; logFC: $\log_2$-transformed fold changes

to their skin counterparts. Of note, differentiation protocols based on EB formation show a lower cardiomyogenic efficiency compared to other up-to-date optimized protocols using, for example, Activin A, BMP4 or chemical inhibitors of Wnt signaling to push cardiomyogenic differentiation (39-41). Nevertheless, we have specifically chosen a standard spontaneous differentiation protocol because the aim of the work was to identify potential differences in cardiomyogenic efficiency between skin and cardiac-derived iPSCs and not to adopt specific measures able to globally increase the cardiomyogenic potential of iPSCs but also potentially capable of abolishing epigenetic-related differences (39-41).

The observation that cardiac iPSCs display better cardiogenic properties even though the original stromal cells are not cardiomyocytes strongly supports the hypothesis that stromal cells could actually act as *in vivo* precursor cells, being able to acquire cardiomyocyte-like properties when exposed to appropriate stimuli (14, 15). This observation is in line with our recent report showing in a rat model of chronic myocardial infarction that isolated adult cardiac stromal cells shared the same morphology and surface markers to bone marrow stromal cells. Nevertheless adult CStCs displayed superior cardiac-specific properties, such as efficient expression of cardiovascular markers *in vitro*, and more proficient integration into the myocardial tissue, as well as cardiomyocyte differentiation after *in vivo* injection, than stromal cells of bone marrow origin (14). In the present work, we also demonstrated that C-iPSCs exhibit a functional memory of the cardiac muscle even if they are obtained from fetal samples. This observation is extremely important when considering that different authors have hypothesized that iPSCs obtained from fetal samples would not retain the same tissue-specific markers as their adult counterparts. Our findings indicate that the tissue of origin actually influences the differentiation abilities of their iPSCs regardless of the developmental stages of founder stromal cells. Of note, fetal CStCs, similar to adult stromal cells, presented a certain degree of plasticity towards the cardiomyocyte phenotype when proper cardiogenic induction is provided (14).

The molecular determinants of the observed functional differences between iPSCs from cells of different origin remain to be determined. A major factor is probably the distinct molecular networks activated or repressed in the two cell populations, among which miRs might play a role. Interestingly, we have recently shown that adult cardiac and bone marrow stromal cells exhibit a specific small subset of miRs whose expression remains unmodified after exposure to diverse differentiation stimuli, thus defining a cell-type specific signature (42). Notably, as previously described for adult stromal cells, also fetal stromal cells exhibited a subset of tissue-specific miRs. Nonetheless, the differences in miR expression observed between fetal CStCs and SStCs were completely abolished by the reprogramming process. However, a deeper analysis revealed that, despite a common core of 91 miRs equally modulated during the pluripotency induction, CStCs and

Table 8. Subset of miRs significantly modulated by the induction of pluripotency in cardiac and skin StCs *vs* iPSCs

Common miRs	Cardiac		Skin	
	iPSCs *vs* StCs		iPSCs *vs* StCs	
	adjP	logFC	adjP	logFC
hsa-miR-367-3p	1.77E-06	15.17	1.49E-06	15.35
hsa-miR-302a-3p	6.72E-06	14.51	5.13E-06	14.97
hsa-miR-302c-3p	1.50E-06	14.27	6.34E-07	15.39
hsa-miR-302b-3p	2.10E-06	13.61	6.46E-07	15.23
hsa-miR-302a-5p	1.16E-07	12.88	2.83E-08	14.42
hsa-miR-302d-3p	3.36E-06	12.88	7.49E-07	14.82
hsa-miR-372-3p	5.94E-08	12.82	1.26E-07	11.75
hsa-miR-512-3p	2.21E-09	12.35	2.28E-09	12.33
hsa-miR-517a-3p	5.92E-09	12.08	5.79E-09	12.09
hsa-miR-517c-3p	6.01E-07	11.01	1.55E-06	9.99
hsa-miR-520g-3p	2.17E-06	10.52	3.25E-06	10.20
hsa-miR-302d-5p	1.42E-08	10.18	7.93E-09	10.60
hsa-miR-302c-5p	2.60E-07	9.98	7.55E-08	11.14
hsa-miR-375	5.07E-07	9.79	1.49E-06	8.66
hsa-miR-200c-3p	1.51E-05	9.45	1.65E-04	7.51
hsa-miR-522-3p	5.25E-06	9.31	4.13E-06	9.59
hsa-miR-183-3p	3.93E-06	8.98	1.87E-05	7.71
hsa-miR-520h	5.32E-07	8.90	3.77E-07	9.13
hsa-miR-302b-5p	4.66E-08	8.80	1.49E-08	9.53
hsa-miR-519d-3p	1.94E-06	8.73	4.46E-07	10.07
hsa-miR-371-3p	4.49E-06	8.59	4.83E-06	8.57
hsa-miR-205-5p	2.28E-04	8.57	1.28E-03	7.15
hsa-miR-525-3p	6.01E-07	8.49	1.26E-07	9.77
hsa-miR-92b-5p	2.60E-07	8.43	1.90E-07	8.53
hsa-miR-223-3p	3.45E-03	8.33	1.79E-02	6.41
hsa-miR-135a-5p	1.14E-04	8.29	2.09E-05	9.72
hsa-miR-20b-5p	6.71E-06	8.21	1.10E-05	7.85
hsa-miR-200a-3p	1.21E-04	8.17	3.98E-05	9.11
hsa-miR-592	1.77E-06	7.83	7.49E-06	6.77
hsa-miR-518e-3p	1.16E-04	7.61	1.02E-04	7.70
hsa-miR-183-5p	1.51E-05	7.57	5.48E-06	8.38
hsa-miR-122-5p	3.88E-05	7.34	5.04E-05	7.13
hsa-miR-515-5p	1.29E-06	7.27	1.55E-06	7.00
hsa-miR-518a-3p	9.01E-06	7.23	1.64E-05	6.85
hsa-miR-520b	1.10E-05	7.11	2.09E-05	6.66
hsa-miR-519b-3p	8.49E-06	7.07	1.29E-05	6.82
hsa-miR-200b-3p	3.86E-03	7.03	3.58E-03	6.98
hsa-miR-512-5p	2.20E-04	6.89	1.47E-03	5.60
hsa-miR-203a	5.88E-04	6.89	3.04E-03	5.58
hsa-miR-605	9.86E-05	6.84	2.03E-04	6.31
hsa-miR-525-5p	4.98E-05	6.52	1.82E-03	4.43
hsa-miR-519c-3p	1.20E-03	6.44	3.18E-03	5.62
hsa-miR-182-5p	2.57E-04	6.30	6.23E-05	7.28
hsa-miR-135b-5p	3.44E-03	6.13	3.58E-03	5.97
hsa-miR-1263	1.67E-05	6.13	5.48E-06	6.85
hsa-miR-141-3p	4.88E-03	5.73	4.31E-02	3.90
hsa-miR-518c-3p	9.92E-04	5.69	1.94E-03	5.20
hsa-miR-515-3p	1.42E-04	5.65	2.09E-05	6.82
hsa-miR-9-5p	4.06E-02	5.57	8.54E-04	9.92
hsa-miR-1251	3.86E-03	5.51	1.29E-02	4.55
hsa-miR-518d-5p	1.62E-03	5.41	1.38E-03	5.52
hsa-miR-18a-5p	8.09E-04	5.39	2.71E-03	4.58
hsa-miR-135b-3p	1.10E-02	5.38	3.25E-03	6.28
hsa-miR-518f-3p	1.99E-02	5.16	3.87E-02	4.44
hsa-miR-520c-3p	1.06E-02	5.10	1.48E-03	6.64
hsa-miR-489-3p	2.20E-04	5.06	1.18E-03	4.24
hsa-miR-20b-3p	9.90E-05	4.92	7.19E-05	5.06
hsa-miR-524-3p	1.28E-05	4.81	1.62E-05	4.73
hsa-miR-363-5p	3.44E-03	4.78	1.58E-04	6.72
hsa-miR-488-5p	9.77E-03	4.61	9.21E-03	4.55
hsa-miR-520f-3p	3.35E-02	4.59	2.87E-02	4.69
hsa-miR-9-3p	4.94E-02	4.57	3.91E-03	6.83
hsa-miR-516b-5p	3.05E-02	4.5.0	1.10E-02	5.26
hsa-miR-548b-5p	1.73E-02	4.46	3.66E-03	5.49
hsa-miR-577	3.25E-03	4.20	1.35E-04	5.95
hsa-miR-106a-5p	1.05E-03	3.94	1.01E-02	2.86
hsa-miR-17-5p	1.34E-03	3.89	1.57E-02	2.73
hsa-miR-429	4.94E-02	3.83	1.32E-03	6.80
hsa-miR-95-3p	2.25E-02	3.77	6.84E-04	6.10
hsa-miR-93-5p	3.86E-03	3.24	4.98E-02	2.06
hsa-miR-19b-3p	1.00E-02	3.19	3.87E-02	2.45
hsa-miR-520e	2.56E-02	2.72	6.53E-03	3.32
hsa-miR-340-3p	3.74E-02	2.07	1.95E-03	3.24
hsa-miR-155-5p	5.86E-03	−2.67	3.34E-05	−4.74
hsa-miR-574-3p	1.19E-03	−3.35	3.57E-04	−3.81
hsa-let-7e-5p	3.18E-02	−3.56	2.87E-02	−3.58

(Cond...)

(Cond...)

Table 8. *(Continued...)*

hsa-miR-654-3p	2.66E-02	−3.83	3.00E-02	−3.68
hsa-miR-193a-5p	9.59E-04	−4.00	2.84E-04	−4.53
hsa-miR-99a-3p	2.84E-02	−4.09	3.25E-03	−5.62
hsa-miR-145-5p	1.16E-02	−4.19	2.54E-02	−3.62
hsa-miR-409-3p	4.94E-02	−4.20	1.41E-02	−5.30
hsa-miR-181c-5p	3.70E-03	−4.25	2.92E-02	−3.03
hsa-let-7b-5p	1.16E-02	−4.75	3.68E-02	−3.80
hsa-miR-432-5p	4.94E-02	−5.01	2.03E-03	−8.35
hsa-miR-100-3p	4.81E-05	−5.30	1.94E-03	−3.54
hsa-miR-770-5p	1.94E-02	−5.32	2.29E-03	−7.18
hsa-miR-424-3p	1.91E-02	−5.40	4.40E-03	−6.59
hsa-miR-137	1.39E-02	−5.62	5.58E-03	−6.34
hsa-miR-100-5p	3.27E-04	−5.67	6.09E-04	−5.34
hsa-miR-493-5p	4.30E-03	−5.90	1.63E-03	−6.69
hsa-miR-99a-5p	5.66E-05	−6.60	1.65E-04	−5.91
Cardiac				
Cardiac-specific miRs	**iPSCs *vs* StCs**			
	adjP	**logFC**		
hsa-miR-504-5p	0.0033	6.98		
hsa-miR-1225-3p	0.0388	6.30		
hsa-miR-142-3p	0.0232	5.76		
hsa-miR-296-3p	0.0040	5.40		
hsa-miR-142-5p	0.0079	5.27		
hsa-miR-449b-5p	0.0057	5.24		
hsa-miR-148a-3p	0.0034	5.20		
hsa-miR-526b-3p	0.0133	5.20		
hsa-miR-139-5p	0.0203	5.18		
hsa-miR-129-2-3p	0.0308	4.66		
hsa-miR-518b	0.0494	4.45		
hsa-miR-20a-5p	0.0066	3.62		
hsa-miR-19a-3p	0.0117	3.14		
hsa-miR-92a-3p	0.0016	3.09		
hsa-miR-106b-5p	0.0099	3.08		
hsa-miR-378a-3p	0.0435	2.94		
hsa-miR-942	0.0358	2.93		
hsa-miR-25-3p	0.0123	2.72		
hsa-miR-18a-3p	0.0430	2.45		
hsa-miR-708-5p	0.0324	2.31		
hsa-miR-550a-3p	0.0266	2.24		
hsa-miR-93-3p	0.0184	2.20		

(Cond...)

Table 8. *(Continued...)*

hsa-miR-218-5p	0.0379	2.01		
hsa-miR-30a-3p	0.0494	−2.34		
hsa-miR-181a-5p	0.0361	−2.71		
hsa-miR-217	0.0494	−3.56		
hsa-miR-181a-2-3p	0.0024	−3.93		
hsa-miR-216a-5p	0.0435	−4.28		
hsa-miR-377-5p	0.0133	−4.54		
hsa-miR-889	0.0358	−4.90		
hsa-miR-1208	0.0335	−4.97		
hsa-miR-21-3p	0.0494	−5.07		
hsa-miR-24-2-5p	0.0161	−5.77		
Skin				
Skin-specific miRs	**iPSCs *vs* StCs**			
	adjP	**logFC**		
hsa-miR-663b	0.0073	10.58		
hsa-miR-1825	0.0022	10.11		
hsa-miR-204-5p	0.0036	7.55		
hsa-miR-1296	0.0448	6.93		
hsa-miR-622	0.0001	6.83		
hsa-miR-767-5p	0.0018	6.73		
hsa-miR-1291	0.0032	5.87		
hsa-miR-519e-5p	0.0010	5.87		
hsa-miR-1298	0.0020	5.82		
hsa-miR-146a-5p	0.0081	5.38		
hsa-miR-184	0.0065	5.33		
hsa-miR-497-5p	0.0025	5.31		
hsa-miR-520a-3p	0.0431	4.98		
hsa-miR-1303	0.0342	4.88		
hsa-miR-1179	0.0205	4.48		
hsa-miR-551b-5p	0.0369	4.20		
hsa-miR-378a-5p	0.0360	3.93		
hsa-miR-96-5p	0.0202	3.25		
hsa-miR-301a-3p	0.0448	3.12		
hsa-miR-126-3p	0.0386	2.96		
hsa-miR-340-5p	0.0355	2.29		
hsa-miR-1290	0.0248	2.07		
hsa-miR-320a	0.0283	−1.93		
hsa-miR-222-3p	0.0016	−2.64		
hsa-miR-193b-3p	0.0037	−2.64		
hsa-miR-138-5p	0.0183	−2.67		

(Cond...)

Table 8. *(Continued...)*

hsa-miR-134-5p	0.0387	−2.68		
hsa-miR-99b-3p	0.0093	−3.39		
hsa-miR-452-5p	0.0036	−3.55		
hsa-miR-450b-5p	0.0450	−3.77		
hsa-miR-98-5p	0.0360	−3.81		
hsa-miR-27a-5p	0.0259	−3.83		
hsa-miR-136-5p	0.0334	−3.83		
hsa-miR-125b-1-3p	0.0450	−4.05		
hsa-miR-541-3p	0.0305	−4.09		
hsa-miR-767-3p	0.0384	−4.85		
hsa-miR-485-3p	0.0305	−5.33		
hsa-miR-655-3p	0.0183	−5.51		
hsa-miR-337-3p	0.0154	−5.64		
hsa-miR-573	0.0305	−5.75		
hsa-miR-337-5p	0.0158	−5.89		
hsa-miR-376c-3p	0.0158	−6.32		
hsa-miR-518c-5p	0.0069	−6.83		
adjP: Benjamini and Hochberg adjusted p-values; logFC: log_2-transformed fold changes				

SStCs still displayed 33 and 43 differentially modulated miRs, respectively as an index and a consequence of their specific response to the reprogramming process. Interestingly, KEGG pathway analysis performed on validated targets revealed that the 33 miRs associated with the reprogramming of CStCs specifically target VEGF and TGF-beta pathways. The role of VEGF in cellular processes that are crucial for cardiac development is well known (43). Also, a recent study demonstrated that VEGF ameliorates the efficiency of differentiation into cardiomyocytes of iPSCs from different somatic origin (44). Additionally, the TGF-beta pathway has been associated to cardiomyogenic-like differentiation of mesenchymal stem cells (MSCs), to cardiosphere formation and maturation and to enhanced cardiogenic potential (45, 46). On the other hand, the HIF-1 signaling pathway, known to reduce the number and the maturation of differentiating cardiomyocytes, is specifically targeted by miRs during the reprogramming process of SStCs. Of note, HIF-1 signaling appears to impair cardiogenic differentiation by reducing the number and the maturation of differentiating cardiomyocytes, which might provide a possible explanation of the lower cardiac differentiation capabilities observed in S-iPSCs (47). Finally, among the commonly targeted pathways, the PI3K/Akt pathway can be involved in the molecular mechanisms regulating cardiomyogenesis specifically by suppressing the GSK-3β activity and maintaining the Wnt/beta-catenin activity (48). Gene-enrichment analysis in GO categories performed on miR validated targets provide further hints of the profound differences in transcriptional regulation between cells of cardiac and skin origin during reprogramming to iPSCs. Of note, some miRs associated with the reprogramming of CStCs specifically target the HDAC binding gene category. It has been shown that HDAC inhibition promotes myocardial repair, prevents cardiac remodeling, and induces the entry of mesodermal cells into the cardiac muscle lineage (49, 50). On the other hand, the overexpression of HDAC4 inhibited cardiomyogenesis and downregulated cardiac muscle gene expression (50). Consistently, higher levels of histone acetylation of H3 and H4 at cardiac-specific gene promoter regions, as well as lower binding levels of HDAC1 and HDAC2, were observed in cardiac stem cells (CSCs) when compared to MSCs, and this reflects a stronger potential for CSCs to develop into cardiomyocytes (51). In our model, the up-regulation of miR-92a-3p in CStCs during reprogramming is associated with a significant reduction of its validated target GCN5 in C-iPSCs compared to S-iPSCs (52). Nevertheless, the level of PCAF acetylase remained unchanged in C- and S-iPSCs, probably due the fact that PCAF can be targeted by several miRs whose expression is modulated in both directions. miR-92a-3p, -19a-3p, -25-3p, and 106b-5p expression was, in fact, up-regulated, while miR-181a-5p was down-regulated during the reprogramming process. Additional experiments are needed to elucidate the mechanistic role of miRs and their targets in determining epigenetic memory in our iPSC model.

Although the molecular mechanisms responsible for this process remain to be characterized in depth, our results support the notion that iPSCs retain a memory of their tissue of origin and, as a consequence, have better cardiac differentiation aptitudes.

6. ACKNOWLEDGEMENTS

This work was supported by Italian Ministry of University (FIRB-MIUR RBFR087JMZ_001 to A.R.), Ministry of Health and Department of Educational Assistance, University and Research of the Autonomous Province of Bolzano, the South Tyrolean Sparkasse Foundation Italian Ministry of Health, young research grant (GR-2009-1530528 to M.M.), California Institute of Regenerative Medicine (CIRM) Grants (RB4-06276) and National Institute of Health grant (RO1 HL105194) to H-S.V.C. The funders had no role in study design, data collection and analysis, decision to publish, or preparation of the manuscript. The authors would like to thank Dr. Silvia Suffredini for her technical support and Dr. Andrew A. Hicks for his critical reading support of our manuscript.

Table 9. Gene-enrichment analysis of experimentally validated targets of miRs differentially expressed in C-iPSCs *vs* CStCs or in S-iPSCs *vs* SStCs

	Tissue	Term	adjP	#genes
KEGG	Cardiac	p53 signaling pathway	2.08E-13	15
		PI3K-Akt signaling pathway	5.80E-10	33
		Cell cycle	1.52E-08	19
		TGF-beta signaling pathway	9.80E-04	9
		Dorso-ventral axis formation	1.95E-02	4
		VEGF signaling pathway	2.30E-02	7
	Skin	Cell cycle	1.20E-14	32
		DNA replication	4.16E-13	14
		NF-kappa B signaling pathway	9.30E-09	19
		p53 signaling pathway	1.68E-07	17
		PI3K-Akt signaling pathway	1.90E-06	46
		HIF-1 signaling pathway	4.74E-06	21
		Toll-like receptor signaling pathway	1.53E-04	17
		Neurotrophin signaling pathway	1.98E-04	19
		Apoptosis	3.20E-04	14
		ErbB signaling pathway	9.91E-04	15
		NOD-like receptor signaling pathway	1.13E-03	12
		Base excision repair	1.77E-03	8
		One carbon pool by folate	1.38E-02	5
		RNA transport	1.68E-02	20
		Focal adhesion	1.69E-02	25
		Mismatch repair	2.31E-02	6
		Insulin signaling pathway	2.34E-02	18
		mTOR signaling pathway	3.81E-02	10
		Adherens junction	4.60E-02	11
BP	Cardiac	Ribosome biogenesis	2.79E-05	39
		Positive regulation of ubiquitin-protein ligase activity during mitotic cell cycle	2.55E-04	25
		Anaphase-promoting complex-dependent proteasomal ubiquitin-dependent protein catabolic process	3.67E-04	24
		rRNA metabolic process	1.96E-03	29
		ER-nuclear signaling pathway	1.20E-02	14
		Dephosphorylation	1.74E-02	37
		RNA export from nucleus	1.81E-02	15
		Negative regulation of cell proliferation	1.84E-02	72
		Regulation of mRNA stability	3.42E-02	10
		Cell morphogenesis involved in differentiation	3.72E-02	51
		Cytoplasmic microtubule organization	4.10E-02	6
	Skin	Regulation of DNA binding	8.71E-06	39
		Regulation of transcription factor activity	1.86E-04	32

(Cond...)

Table 9. *(Continued...)*

	Tissue	Term	adjP	#genes
		Positive regulation of NF-kappaB transcription factor activity	2.52E-04	18
		Cell migration	6.14E-04	62
		Actin filament-based process	3.61E-03	53
		DNA duplex unwinding	4.77E-03	10
		Protein heterooligomerization	5.35E-03	18
		Epithelial tube morphogenesis	5.81E-03	21
		Response to cytokine stimulus	8.03E-03	23
		Positive regulation of protein kinase cascade	8.07E-03	39
		Senescence	1.45E-02	6
		Protein export from nucleus	2.19E-02	9
		Androgen receptor signaling pathway	2.80E-02	13
		Positive regulation of fatty acid oxidation	3.02E-02	6
		Leukocyte cell-cell adhesion	3.76E-02	11
		Spliceosomal snRNP biogenesis	3.76E-02	11
		DNA replication initiation	4.57E-02	8
		Intracellular receptor-mediated signaling pathway	4.90E-02	20
MF	Cardiac	RNA helicase activity	1.57E-02	13
		Histone deacetylase binding	2.36E-02	13
		Translation elongation factor activity	3.32E-02	11
		Phosphatase activity	3.78E-02	53
		Protein C-terminus binding	4.44E-02	34
	Skin	Helicase activity	8.45E-04	38
		Protein complex binding	2.40E-02	43
		DNA-dependent ATPase activity	2.60E-02	18
		Histone binding	3.40E-02	15
		Ligand-dependent nuclear receptor transcription coactivator activity	4.35E-02	13
		Nitric-oxide synthase regulator activity	4.49E-02	5

adjP: Benjamini and hochberg adjusted p-values; KEGG: KEGG pathways; BP: GO biological process; MF: GO Molecular function

7. REFERENCES

1. H. Inoue, and S. Yamanaka: The use of induced pluripotent stem cells in drug development. *Clin Pharmacol Ther* 89, 655-661 (2011) DOI: 10.1038/clpt.2011.38
2. M. Z. Chow, K. R. Boheler, and R. A. Li: Human pluripotent stem cell-derived cardiomyocytes for heart regeneration, drug discovery and disease modeling: from the genetic, epigenetic, and tissue modeling perspectives. *Stem Cell Res Ther* 4, (4):97 (2013) DOI: 10.1186/scrt308
3. K. Takahashi, K. Tanabe, M. Ohnuki, M. Narita, T. Ichisaka, K. Tomoda, and S. Yamanaka: Induction of pluripotent stem cells from adult human fibroblasts by defined factors. *Cell* 131, 861-872 (2007) DOI: 10.1016/j.cell.2007.11.019
4. K. Okita, T. Yamakawa, Y. Matsumura, Y. Sato, N. Amano, A. Watanabe, N. Goshima, and S. Yamanaka: An efficient nonviral method to generate integration-free human-induced pluripotent stem cells from cord blood and peripheral blood cells. *Stem Cells* 31, 458-466 (2013) DOI: 10.1002/stem.1293

5. K. Kim, R. Zhao, A. Doi, K. Ng, J. Unternaehrer, P. Cahan, H. Huo, Y. H. Loh, M. J. Aryee, M. W. Lensch, H. Li, J. J. Collins, A. P. Feinberg, and G. Q. Daley: Donor cell type can influence the epigenome and differentiation potential of human induced pluripotent stem cells. *Nat Biotechnol* 29, 1117-1119 (2011)
DOI: 10.1038/nbt.2052

6. K. Streckfuss-Bömeke, F. Wolf, A. Azizian, M. Stauske, M. Tiburcy, S. Wagner, D. Hübscher, R. Dressel, S. Chen, J. Jende, G. Wulf, V. Lorenz, M. P. Schön, L. S. Maier, W. H. Zimmermann, G. Hasenfuss, K. Guan: Comparative study of human-induced pluripotent stem cells derived from bone marrow cells, hair keratinocytes, and skin fibroblasts. Eur Heart J 34, 2618-2629 (2013)
DOI: 10.1093/eurheartj/ehs203

7. N. Miyoshi, H. Ishii, H. Nagano, N. Haraguchi, D. L. Dewi, Y. Kano, S. Nishikawa, M. Tanemura, K. Mimori, F. Tanaka, T. Saito, J. Nishimura, I. Takemasa, T. Mizushima, M. Ikeda, H. Yamamoto, M. Sekimoto, Y. Doki, and M. Mori: Reprogramming of mouse and human cells to pluripotency using mature microRNAs. *Cell stem cell* 8, 633-638 (2011)
DOI: 10.1016/j.stem.2011.05.001

8. I. Petit, N. S. Kesner, R. Karry, O. Robicsek, E. Aberdam, F. J. Muller, D. Aberdam, and D. Ben-Shachar: Induced pluripotent stem cells from hair follicles as a cellular model for neurodevelopmental disorders. *Stem Cell Res* 8, 134-140 (2012) 10.1.016/j.scr.2011.0.9.0.03
DOI: 10.1016/j.scr.2011.09.003

9. P. C. Beltrao-Braga, G. C. Pignatari, P. C. Maiorka, N. A. Oliveira, N. F. Lizier, C. V. Wenceslau, M. A. Miglino, A. R. Muotri, and I. Kerkis: Feeder-free derivation of induced pluripotent stem cells from human immature dental pulp stem cells. *Cell Transplant* 20, 1707-1719 (2011)
DOI: 10.3727/096368911X566235

10. N. Maherali, R. Sridharan, W. Xie, J. Utikal, S. Eminli, K. Arnold, M. Stadtfeld, R. Yachechko, J. Tchieu, R. Jaenisch, K. Plath, and K. Hochedlinger: Directly reprogrammed fibroblasts show global epigenetic remodeling and widespread tissue contribution. *Cell Stem Cell* 1, 55-70 (2007)
DOI: 10.1016/j.stem.2007.05.014

11. R. Rizzi, E. Di Pasquale, P. Portararo, R. Papait, P. Cattaneo, M. V. Latronico, C. Altomare, L. Sala, A. Zaza, E. Hirsch, L. Naldini, G. Condorelli, and C. Bearzi: Post-natal cardiomyocytes can generate iPS cells with an enhanced capacity toward cardiomyogenic re-differentation. *Cell Death Differ* 19, 1162-1174 (2012)
DOI: 10.1038/cdd.2011.205

12. H. Xu, B. A. Yi, H. Wu, C. Bock, H. Gu, K. O. Lui, J. H. Park, Y. Shao, A. K. Riley, I. J. Domian, E. Hu, R. Willette, J. Lepore, A. Meissner, Z. Wang, and K. R. Chien: Highly efficient derivation of ventricular cardiomyocytes from induced pluripotent stem cells with a distinct epigenetic signature. *Cell Res* 22, 142-154 (2012)
DOI: 10.1038/cr.2011.171

13. V. Sanchez-Freire, A. S. Lee, S. Hu, O. J. Abilez, P. Liang, F. Lan, B. C. Huber, S. G. Ong, W. X. Hong, M. Huang, and J. C. Wu: Effect of human donor cell source on differentiation and function of cardiac induced pluripotent stem cells. *J Am Coll Cardiol* 64, 436-448 (2014)
DOI: 10.1016/j.jacc.2014.04.056

14. A. Rossini, C. Frati, C. Lagrasta, G. Graiani, A. Scopece, S. Cavalli, E. Musso, M. Baccarin, M. Di Segni, F. Fagnoni, A. Germani, E. Quaini, M. Mayr, Q. Xu, A. Barbuti, D. DiFrancesco, G. Pompilio, F. Quaini, C. Gaetano, and M. C. Capogrossi: Human cardiac and bone marrow stromal cells exhibit distinctive properties related to their origin. *Cardiovasc research* 89, 650-60 (2011)
DOI: 10.1093/cvr/cvq290

15. M. Vecellio, V. Meraviglia, S. Nanni, A. Barbuti, A. Scavone, D. DiFrancesco, A. Farsetti, G. Pompilio, G. I. Colombo, M. C. Capogrossi, C. Gaetano, and A. Rossini: *In vitro* epigenetic reprogramming of human cardiac mesenchymal stromal cells into functionally competent cardiovascular precursors. *PLoS One* 7, e51694 (2012)
DOI: 10.1371/journal.pone.0051694

16. M. Vecellio, F. Spallotta, S. Nanni, C. Colussi, C. Cencioni, A. Derlet, B. Bassetti, M. Tilenni, M. C. Carena, A. Farsetti, G. Sbardella, S. Castellano, A. Mai, F. Martelli, G. Pompilio, M. C. Capogrossi, A. Rossini, S. Dimmeler, A. M. Zeiher, and C. Gaetano: The Histone

Acetylase Activator Pentadecylidenemalonate 1b Rescues Proliferation and Differentiation in Human Cardiac Mesenchymal Cells of Type 2 Diabetic Patients. *Diabetes* 63, 2132-2147 (2014)
DOI: 10.2337/db13-0731

17. K. Okita, Y. Matsumura, Y. Sato, A. Okada, A. Morizane, S. Okamoto, H. Hong, M. Nakagawa, K. Tanabe, K. Tezuka, T. Shibata, T. Kunisada, M. Takahashi, J. Takahashi, H. Saji, and S. Yamanaka: A more efficient method to generate integration-free human iPS cells. *Nat Methods* 8, 409-412 (2011)
DOI: 10.1038/nmeth.1591

18. V. Meraviglia, A. Zanon, A. A. Lavdas, C. Schwienbacher, R. Silipigni, M. Di Segni, H. S. Chen, P. P. Pramstaller, A. A. Hicks, and A. Rossini: Generation of Induced Pluripotent Stem Cells from Frozen Buffy Coats using Non-integrating Episomal Plasmids. *J Vis Exp* 100, e52885 (2015)
DOI: 10.3791/52885

19. C. Kim, M. Majdi, P. Xia, K. A. Wei, M. Talantova, S. Spiering, B. Nelson, M. Mercola, and H. S. Chen: Non-cardiomyocytes influence the electrophysiological maturation of human embryonic stem cell-derived cardiomyocytes during differentiation. *Stem Cells Dev* 19, 783-795 (2010)
DOI: 10.1089/scd.2009.0349

20. A. Barbuti, A. Crespi, D. Capilupo, N. Mazzocchi, M. Baruscotti, and D. DiFrancesco: Molecular composition and functional properties of f-channels in murine embryonic stem cell-derived pacemaker cells. *J Mol Cell Cardiol* 46, 343-351 (2009)
DOI: 10.1016/j.yjmcc.2008.12.001

21. L. Fassina, A. Di Grazia, F. Naro, L. Monaco, M. G. De Angelis, and G. Magenes: Video evaluation of the kinematics and dynamics of the beating cardiac syncytium: an alternative to the Langendorff method. *Int J Artif Organs* 34, 546-558 (2011)
DOI: 10.5301/IJAO.2011.8510

22. K. J. Livak, and T. D. Schmittgen: Analysis of relative gene expression data using real-time quantitative PCR and the 2(-Delta Delta C(T)) Method. *Methods* 25, 402-408 (2001)
DOI: 10.1006/meth.2001.1262

23. S. Griffiths-Jones, H. K. Saini, S. van Dongen, and A. J. Enright: miRBase: tools for microRNA genomics. *Nucleic Acids Res* 36, D154-8 (2008)
DOI: 10.1093/nar/gkm952

24. P. Mestdagh, P. Van Vlierberghe, A. De Weer, D. Muth, F. Westermann, F. Speleman, and J. Vandesompele: A novel and universal method for microRNA RT-qPCR data normalization. *Genome Biol* 10, R64 (2009)
DOI: 10.1186/gb-2009-10-6-r64

25. G. K. Smyth: Linear models and empirical bayes methods for assessing differential expression in microarray experiments. *Stat Appl Genet Mol Biol* 3, Article3 (2004)
(No DOI Found)

26. A. I. Saeed, V. Sharov, J. White, J. Li, W. Liang, N. Bhagabati, J. Braisted, M. Klapa, T. Currier, M. Thiagarajan, A. Sturn, M. Snuffin, A. Rezantsev, D. Popov, A. Ryltsov, E. Kostukovich, I. Borisovsky, Z. Liu, A. Vinsavich, V. Trush, and J. Quackenbush: TM4: a free, open-source system for microarray data management and analysis. *BioTechniques* 34, 374-378 (2003)
(No DOI Found)

27. T. Vergoulis, I. S. Vlachos, P. Alexiou, G. Georgakilas, M. Maragkakis, M. Reczko, S. Gerangelos, N. Koziris, T. Dalamagas, and A. G. Hatzigeorgiou: TarBase 6.0.: capturing the exponential growth of miRNA targets with experimental support. *Nucleic Acids Res* 40, D222-229 (2012)
DOI: 10.1093/nar/gkr1161

28. S. D. Hsu, F. M. Lin, W. Y. Wu, C. Liang, W. C. Huang, W. L. Chan, W. T. Tsai, G. Z. Chen, C. J. Lee, C. M. Chiu, C. H. Chien, M. C. Wu, C. Y. Huang, A. P. Tsou, and H. D. Huang: miRTarBase: a database curates experimentally validated microRNA-target interactions. *Nucleic Acids Res* 39, D163-169 (2011)
DOI: 10.1093/nar/gkq1107

29. I. S. Vlachos, N. Kostoulas, T. Vergoulis, G. Georgakilas, M. Reczko, M. Maragkakis, M. D. Paraskevopoulou, K. Prionidis, T. Dalamagas, and A. G. Hatzigeorgiou: DIANA miRPath v.2.0.: investigating the combinatorial effect of microRNAs in pathways. *Nucleic Acids Res* 40, W498-504 (2012)
DOI: 10.1093/nar/gks494

30. W. Huang da, B. T. Sherman, and R. A. Lempicki: Systematic and integrative analysis

of large gene lists using DAVID bioinformatics resources. *Nat Protoc* 4, 44-57 (2009)
DOI: 10.1038/nprot.2008.211

31. F. Supek, M. Bosnjak, N. Skunca, and T. Smuc: REVIGO summarizes and visualizes long lists of gene ontology terms. *PLoS One* 6, e21800 (2011)
DOI: 10.1371/journal.pone.0021800

32. J. J. Montesinos, E. Flores-Figueroa, S. Castillo-Medina, P. Flores-Guzman, E. Hernandez-Estevez, G. Fajardo-Orduna, S. Orozco, and H. Mayani: Human mesenchymal stromal cells from adult and neonatal sources: comparative analysis of their morphology, immunophenotype, differentiation patterns and neural protein expression. *Cytotherapy* 11, 163-176 (2009)
DOI: 10.1080/14653240802582075

33. M. Crisan, S. Yap, L. Casteilla, C. W. Chen, M. Corselli, T. S. Park, G. Andriolo, B. Sun, B. Zheng, L. Zhang, C. Norotte, P. N. Teng, J. Traas, R. Schugar, B. M. Deasy, S. Badylak, H. J. Buhring, J. P. Giacobino, L. Lazzari, J. Huard, and B. Peault: A perivascular origin for mesenchymal stem cells in multiple human organs. *Cell Stem Cell* 3, 301-313 (2008)
DOI: 10.1016/j.stem.2008.07.003

34. F. Di Meglio, D. Nurzynska, C. Castaldo, A. Arcucci, L. De Santo, M. de Feo, M. Cotrufo, S. Montagnani, and G. Giordano-Lanza: *In vitro* cultured progenitors and precursors of cardiac cell lineages from human normal and post-ischemic hearts. *Eur J Histochem* 51, 275-282 (2007)
(No DOI Found)

35. K. Kim, A. Doi, B. Wen, K. Ng, R. Zhao, P. Cahan, J. Kim, M. J. Aryee, H. Ji, L. I. Ehrlich, A. Yabuuchi, A. Takeuchi, K. C. Cunniff, H. Hongguang, S. McKinney-Freeman, O. Naveiras, T. J. Yoon, R. A. Irizarry, N. Jung, J. Seita, J. Hanna, P. Murakami, R. Jaenisch, R. Weissleder, S. H. Orkin, I. L. Weissman, A. P. Feinberg, and G. Q. Daley: Epigenetic memory in induced pluripotent stem cells. *Nature* 467, 285-290 (2010)
DOI: 10.1038/nature09342

36. M. H. Chin, M. J. Mason, W. Xie, S. Volinia, M. Singer, C. Peterson, G. Ambartsumyan, O. Aimiuwu, L. Richter, J. Zhang, I. Khvorostov, V. Ott, M. Grunstein, N. Lavon, N. Benvenisty, C. M. Croce, A. T. Clark, T. Baxter, A. D. Pyle, M. A. Teitell, M. Pelegrini, K. Plath, and W. E. Lowry: Induced pluripotent stem cells and embryonic stem cells are distinguished by gene expression signatures. *Cell Stem Cell* 5, 111-123 (2009)
DOI: 10.1016/j.stem.2009.06.008

37. Q. Hu, A. M. Friedrich, L. V. Johnson, and D. O. Clegg: Memory in induced pluripotent stem cells: reprogrammed human retinal-pigmented epithelial cells show tendency for spontaneous redifferentiation. *Stem Cells* 28, 1981-1991 (2010)
DOI: 10.1002/stem.531

38. J. A. Mills, K. Wang, P. Paluru, L. Ying, L. Lu, A. M. Galvao, D. Xu, Y. Yao, S. K. Sullivan, L. M. Sullivan, H. Mac, A. Omari, J. C. Jean, S. Shen, A. Gower, A. Spira, G. Mostoslavsky, D. N. Kotton, D. L. French, M. J. Weiss, and P. Gadue: Clonal genetic and hematopoietic heterogeneity among human-induced pluripotent stem cell lines. *Blood* 122, 2047-2051 (2013)
DOI: 10.1182/blood-2013-02-484444

39. X. Q. Xu, R. Graichen, S. Y. Soo, T. Balakrishnan, S. N. Rahmat, S. Sieh, S. C. Tham, C. Freund, J. Moore, C. Mummery, A. Colman, R. Zweigerdt, and B. P. Davidson: Chemically defined medium supporting cardiomyocyte differentiation of human embryonic stem cells. *Differentiation* 76, 958-970 (2008)
DOI: 10.1111/j.1432-0436.2008.00284.x

40. S. J. Kattman, A. D. Witty, M. Gagliardi, N. C. Dubois, M. Niapour, A. Hotta, J. Ellis, and G. Keller: Stage-specific optimization of activin/nodal and BMP signaling promotes cardiac differentiation of mouse and human pluripotent stem cell lines. *Cell Stem Cell* 8, 228-240 (2011)
DOI: 10.1016/j.stem.2010.12.008

41. X. Lian, C. Hsiao, G. Wilson, K. Zhu, L. B. Hazeltine, S. M. Azarin, K. K. Raval, J. Zhang, T. J. Kamp, and S. P. Palecek: Robust cardiomyocyte differentiation from human pluripotent stem cells via temporal modulation of canonical Wnt signaling. *Proc Natl Acad Sci U S A* 109, E1848-1857 (2012)
DOI: 10.1073/pnas.1200250109

42. V. Meraviglia, V. Azzimato, L. Piacentini, M. Chiesa, R. K. Kesharwani, C. Frati, M. C. Capogrossi, C. Gaetano, G. Pompilio, G. I.

Colombo, and A. Rossini: Syngeneic cardiac and bone marrow stromal cells display tissue-specific microRNA signatures and microRNA subsets restricted to diverse differentiation processes. *PLoS One* 9, e107269 (2014) DOI: 10.1371/journal.pone.0107269

43. N. M. van den Akker, V. Caolo, and D. G. Molin: Cellular decisions in cardiac outflow tract and coronary development: an act by VEGF and NOTCH. *Differentiation* 84, 62-78 (2012) DOI: 10.1016/j.diff.2012.04.002

44. L. Ye, S. Zhang, L. Greder, J. Dutton, S. A. Keirstead, M. Lepley, L. Zhang, D. Kaufman, and J. Zhang: Effective cardiac myocyte differentiation of human induced pluripotent stem cells requires VEGF. *PLoS One* 8, e53764 (2013) DOI: 10.1371/journal.pone.0053764

45. S. Mohanty, S. Bose, K. G. Jain, B. Bhargava, and B. Airan: TGFbeta1 contributes to cardiomyogenic-like differentiation of human bone marrow mesenchymal stem cells. *Int J Cardiol* 163, 93-99 (2013) DOI: 10.1016/j.ijcard.2011.08.003

46. E. Forte, F. Miraldi, I. Chimenti, F. Angelini, A. Zeuner, A. Giacomello, M. Mercola, and E. Messina: TGFbeta-dependent epithelial-to-mesenchymal transition is required to generate cardiospheres from human adult heart biopsies. *Stem Cells Dev* 21, 3081-3090 (2012) DOI: 10.1089/scd.2012.0277

47. T. L. Medley, M. Furtado, N. T. Lam, R. Idrizi, D. Williams, P. J. Verma, M. Costa, and D. M. Kaye: Effect of oxygen on cardiac differentiation in mouse iPS cells: role of hypoxia inducible factor-1 and Wnt/beta-catenin signaling. *PLoS One* 8, e80280 (2013) DOI: 10.1371/journal.pone.0080280

48. A. T. Naito, H. Akazawa, H. Takano, T. Minamino, T. Nagai, H. Aburatani, and I. Komuro: Phosphatidylinositol 3-kinase-Akt pathway plays a critical role in early cardiomyogenesis by regulating canonical Wnt signaling. *Circ Res* 97, 144-151 (2005) DOI: 10.1161/01.RES.0000175241.92285.f8

49. L. Zhang, B. Chen, Y. Zhao, P. M. Dubielecka, L. Wei, G. J. Qin, Y. E. Chin, Y. Wang, and T. C. Zhao: Inhibition of histone deacetylase-induced myocardial repair is mediated by c-kit in infarcted hearts. *J Biol Chem* 287, 39338-39348 (2012) DOI: 10.1074/jbc.M112.379115

50. C. Karamboulas, A. Swedani, C. Ward, A. S. Al-Madhoun, S. Wilton, S. Boisvenue, A. G. Ridgeway, and I. S. Skerjanc: HDAC activity regulates entry of mesoderm cells into the cardiac muscle lineage. *J Cell Sci* 119, 4305-4314 (2006) DOI: 10.1242/jcs.03185

51. M. Wang, Q. Yu, L. Wang, and H. Gu: Distinct patterns of histone modifications at cardiac-specific gene promoters between cardiac stem cells and mesenchymal stem cells. *Am J Physiol Cell Physiol* 304, C1080-C1090 (2013) DOI: 10.1152/ajpcell.00359.2012

52. A. Helwak, G. Kudla, T. Dudnakova, and D. Tollervey: Mapping the human miRNA interactome by CLASH reveals frequent noncanonical binding. *Cell* 153, 654-665 (2013) DOI: 10.1016/j.cell.2013.03.043

Abbreviations: iPSCs: induced pluripotent stem cells; StCs: mesenchymal stromal cells; CStCs: cardiac stromal cells; SStCs: skin stromal cells; C-iPSCs: iPSCs derived from CStCs; S-iPSCs: iPSCs derived from SStCs; miR: microRNA; hESCs: human embryonic stem cells; EBs: embryoid bodies.

Key Words: Induced Pluripotent Stem Cells, Stromal Cells, Fibroblasts, Cardiomyogenic Differentiation, Cardiomyocytes

Send correspondence to: Alessandra Rossini, Dipartimento di Scienze Cliniche e di Comunita, Universita degli Studi di Milano, via Commenda 9/12, 20122, Milano, Italy, and Center for Biomedicine, European Academy Bozen/Bolzano (EURAC) (affiliated institute of the University of Lubeck), Via Galvani 31, I-39100, Bolzano, Italy, Tel: 39 0471 055 504, Fax: 39 0471 055 599, E-mail: alessandra.rossini@eurac.edu